DISTANCE SCALE ZERO POINTS FROM GALACTIC RR LYRAE STAR PARALLAXES[*]

G. Fritz Benedict[1], Barbara E. McArthur[1], Michael W. Feast[2,3], Thomas G. Barnes[1], Thomas E. Harrison[4,16],
Jacob L. Bean[5,17], John W. Menzies[3], Brian Chaboyer[6], Luca Fossati[7], Nicole Nesvacil[8,9], Horace A. Smith[10],
Katrien Kolenberg[5,8], C. D. Laney[3,11], Oleg Kochukhov[12], Edmund P. Nelan[13], D. V. Shulyak[14],
Denise Taylor[13], and Wendy L. Freedman[15]

[1] McDonald Observatory, University of Texas, Austin, TX 78712, USA
[2] Centre for Astrophysics, Cosmology and Gravitation, Astronomy Department, University of Cape Town, Rondebosch 7701, South Africa
[3] South African Astronomical Observatory, Observatory 7935, South Africa
[4] Department of Astronomy, New Mexico State University, Las Cruces, NM 88003, USA
[5] Harvard-Smithsonian Center for Astrophysics, Cambridge, MA 02138, USA
[6] Department of Physics and Astronomy, Dartmouth College, Hanover, NH 03755, USA
[7] Department of Physics and Astronomy, Open University, Milton Keynes MK7 6AA, UK
[8] Institute of Astronomy, University of Vienna, A-1180 Vienna, Austria
[9] Department of Radiotherapy, Medical University of Vienna, A-1090 Vienna, Austria
[10] Department of Physics & Astronomy, Michigan State University, East Lansing, MI 48824, USA
[11] Department of Physics and Astronomy, Brigham Young University, Provo, UT 84602, USA
[12] Department of Physics and Astronomy, Uppsala University, 75120 Uppsala, Sweden
[13] STScI, Baltimore, MD 21218, USA
[14] Institute of Astrophysics, Georg-August-University, Friedrich-Hund-Platz 1, D-37077 Göttingen, Germany
[15] The Observatories, Carnegie Institution of Washington, Pasadena, CA 91101, USA

ABSTRACT

We present new absolute trigonometric parallaxes and proper motions for seven Population II variable stars—five RR Lyr variables: RZ Cep, XZ Cyg, SU Dra, RR Lyr, and UV Oct; and two type 2 Cepheids: VY Pyx and κ Pav. We obtained these results with astrometric data from Fine Guidance Sensors, white-light interferometers on *Hubble Space Telescope*. We find absolute parallaxes in milliseconds of arc: RZ Cep, 2.12 ± 0.16 mas; XZ Cyg, 1.67 ± 0.17 mas; SU Dra, 1.42 ± 0.16 mas; RR Lyr, 3.77 ± 0.13 mas; UV Oct, 1.71 ± 0.10 mas; VY Pyx, 6.44 ± 0.23 mas; and κ Pav, 5.57 ± 0.28 mas; an average $\sigma_\pi / \pi = 5.4\%$. With these parallaxes, we compute absolute magnitudes in V and K bandpasses corrected for interstellar extinction and Lutz–Kelker–Hanson bias. Using these RR Lyrae variable star absolute magnitudes, we then derive zero points for M_V–[Fe/H] and M_K–[Fe/H]–$\log P$ relations. The technique of reduced parallaxes corroborates these results. We employ our new results to determine distances and ages of several Galactic globular clusters and the distance of the Large Magellanic Cloud. The latter is close to that previously derived from Classical Cepheids uncorrected for any metallicity effect, indicating that any such effect is small. We also discuss the somewhat puzzling results obtained for our two type 2 Cepheids.

Key words: astrometry – stars: distances – stars: variables: RR Lyrae

Online-only material: color figures

1. INTRODUCTION

RR Lyrae variable stars (RRLs) have long played a crucial role in understanding old stellar populations (Population II). Paraphrasing Smith (1995), they are important as tracers of the chemical and dynamical properties of old populations, as standard candles in our own and nearby galaxies, and as a test bed for the understanding of stellar pulsation and evolution. Their luminosities are of great potential importance in estimating the distances and hence the ages of globular clusters—both the absolute ages and the relative ages as a function of metallicity, [Fe/H]. An error in distance modulus of 0.1 mag corresponds to an age uncertainty of 1 Gyr. The RRLs are also vital for studies of the structure and formation of our Galaxy, Local Group members, and other nearby galaxies, a field which is currently referred to as Near-Field Cosmology. Their importance as distance indicators comes from the fact that they follow $M(V)$–[Fe/H] and K–$\log P$ or K–[Fe/H]–$\log P$ relations. The zero points of these relations have been much discussed. Trigonometric parallaxes remain the only fundamental method of getting RRL distances and luminosities, free of the assumptions that go into other methods discussed in Section 6.3 below. Absolute parallaxes allow these assumptions to be tested. What is required is an improved fundamental zero-point calibration, which currently rests on the *Hubble Space Telescope* (*HST*) parallax (Benedict et al. 2002b) of RR Lyrae alone (cf. Sollima et al. 2006). In this paper, we apply the astrometric precision of *HST*/FGS to the determination of absolute parallaxes for five galactic RRLs: XZ Cyg = Hip 96112; UV Oct = Hip 80990; RZ Cep = Hip 111839; SU Dra = Hip 56734; RR Lyr = Hip 95497; and two type 2 Cepheids, κ Pav = Hip 93015 and VY Pyx = Hip 43736. Target properties are given in Table 1 and discussed in Section 2.

Type 2 Cepheids (hereafter CP2), more luminous than the RR Lyraes, have great potential as distance indicators in old populations. They have recently been shown to define a narrow K-band period–luminosity relation (PLR; Matsunaga et al. 2006,

Table 1
Target Properties

ID	log P	T_0	$\langle V \rangle$	$\langle K_S \rangle$[a]	[Fe/H][b]	A_V	A_K
RZ Cep (c)[c]	−0.51052	54793.0050	9.47	8.11	−1.77 ± 0.2	0.78	
XZ Cyg (ab)[d]	−0.33107	54395.1020	9.68	8.72	−1.44 0.2	0.30	0.04
SU Dra (ab)[e]	−0.18018	54733.1510	9.78	8.62	−1.80 0.2	0.03	0.00
RR Lyr (ab)[f]	−0.24655	50749.2380	7.76	6.49	−1.41 0.13	0.13	0.01
UV Oct (ab)[g]	−0.26552	53570.4141	9.50	8.30	−1.47 0.11	0.28	0.03
VY Pyx (BLHer)[h]	0.09340	54406.4072	7.30	5.72	−0.01 0.15	0.15	0.02
κ Pav (WVir)[i]	0.95815	54705.9320	4.35	2.78	0.0 0.13	0.05	0.0

Notes.
[a] K_S from Feast et al. (2008), except where noted.
[b] [Fe/H] on the Zinn & West (1984) scale.
[c] RZ Cep: T_0, Smith for this paper; [Fe/H], A_V, Fernley et al. (1998b).
[d] XZ Cyg: Fernley et al. (1998b), Feast et al. (2008); log P, T_0 from LaCluyzé et al. (2004).
[e] SU Dra: Fernley et al. (1998b), Feast et al. (2008).
[f] RR Lyr: Fernley et al. (1998b), Feast et al. (2008); [Fe/H], A_V: Kolenberg et al. (2010).
[g] UV Oct: Fernley et al. (1998b), Feast et al. (2008); log P, T_0 from FGS photometry; [Fe/H] derived as for RR Lyr for this paper.
[h] VY Pyx: Feast et al. (2008); $\langle K_S \rangle$ from Laney for this paper; T_0 from FGS photometry; [Fe/H] derived as for RR Lyr for this paper.
[i] κ Pav: Feast et al. (2008); T_0 from FGS photometry; [Fe/H], Luck & Bond (1989).

2009) with little metallicity dependence. The slope and zero point of this relation are indistinguishable from that of the RRL derived by Sollima et al. (2006). Two CP2s, κ Pavonis and VY Pyxidis (confirmed as such by Zakrzewski et al. 2000), were expected to be sufficiently close that very accurate parallaxes and absolute magnitudes could be obtained with *HST*. Not only could these parallaxes, likely a factor of three more precise than from *Hipparcos*, provide an accurate zero point for the CP2 PLR, but they may facilitate the derivation of the slope and zero point of a combined RRL and CP2 PLR. Majaess (2010) has recently asserted that CP2 and RRL define a single-slope PLR when a Wesenheit magnitude, $W_{VI} = V - 2.45(V - I)$, is plotted against log P.

In the following sections we describe our astrometry using one of our targets, κ Pav, as an example throughout. This longest-period member of our sample has been identified as a peculiar W Vir star (Feast et al. 2008) but, if included, could anchor our K-band PLR slope. Hence, its parallax value deserves as much external scrutiny as possible. We discuss (Section 2) data acquisition and analysis; present the results of spectrophotometry of the astrometric reference stars required to correct our relative parallax to absolute (Section 3); derive absolute parallaxes for these variable stars (Section 4); derive absolute magnitudes (Section 5); determine (Section 6) a K-band PLR zero point and an M_V–[Fe/H] relation zero point, and compare our resulting absolute magnitudes with past determinations; and in Section 7 discuss the distance scale ramifications of our results, and apply our PLR zero points to two interesting classes of object—Globular Clusters (M3, M4, M15, M68, ω Cen, and M92) and the Large Magellanic Cloud (LMC). In Section 8 we discuss the puzzling results for VY Pyx and κ Pav. We summarize our findings in Section 9.

2. OBSERVATIONS AND DATA REDUCTION

Nelan (2010) provides an overview of the Fine Guidance Sensor (FGS) instrument (a two-axis shearing interferometer), and Benedict et al. (2007) describe the fringe tracking (POS) mode astrometric capabilities of an FGS, along with the data acquisition and reduction strategies also used in the present

study. We time-tag our data with a Modified Julian Date, MJD = JD −2400000.5.

Between 13 and 23 sets of astrometric data were acquired with *HST* FGS 1r for each of our 7 science targets. We obtained most of these sets at epochs determined by field availability, primarily dictated by two-gyro guiding constraints. See Benedict et al. (2010) for a brief discussion of these constraints. The various complete data aggregates span from 2.37 to 13.14 years. Table 2 contains the epochs of observation, pulsational phase, the V magnitude, and estimated $B - V$ color index (required for the lateral color correction discussed in Section 4.1) for each variable. The $B - V$ colors are inferred from phased color curves constructed from various sources: XZ Cyg (Sturch 1966), RZ Cep (Epps & Sinclair 1973), SU Dra (Barcza 2002), RR Lyr (Hardie 1955), UV Oct (K. Kolenberg 2010, private communication), κ Pav (Shobbrook 1992), and VY Pyx (Sanwal & Sarma 1991).

Each individual *HST* data set required approximately 33 minutes of spacecraft time. The data were reduced and calibrated as detailed in McArthur et al. (2001), Benedict et al. (2002a, 2002b), Soderblom et al. (2005), and Benedict et al. (2007). At each epoch we measured reference stars and the target multiple times to correct for intra-orbit drift of the type seen in the cross-filter calibration data shown in Figure 1 of Benedict et al. (2002a). The distribution of reference stars on a second generation Digital Sky Survey R image near each of our science targets is shown in Figure 1. The orientation of each successive observation changes, mandated by *HST* solar panel illumination constraints.

Data are downloaded from the *HST* archive and passed through a pipeline processing system. This pipeline extracts the astrometry measurements (typically one to two minutes of fringe x and y position information acquired at a 40 Hz rate, which yields several thousand discrete measurements), extracts the median (which we have found to be the optimum estimator of position), corrects for the Optical Field Angle Distortion (McArthur et al. 2002), and attaches all required time tags and parallax factors.

Table 1 collects measured properties for our target variables, including stellar type (ab or c for RRL), log of the pulsational

Table 2
Log of Observations, Apparent Magnitude, Estimated $B − V$, and Pulsational Phase

Set	MJD	V	$B − V$[a]	Phase	Set	MJD	V	$B − V$[a]	Phase
RZ Cep					XZ Cyg				
1	54287.60885	9.759	0.53	0.6121	1	54292.22174	10.092	0.40	0.5050
1	54287.62167	9.719	0.52	0.6536	1	54292.2351	10.129	0.40	0.5106
1	54287.63148	9.704	0.52	0.6854	1	54292.24162	10.115	0.41	0.5337
1	54287.6403	9.683	0.51	0.7140	1	54292.24659	10.126	0.41	0.5476
1	54287.65023	9.643	0.50	0.7462	2	54322.03022	9.976	0.38	0.3911
1	54287.65756	9.599	0.49	0.7699	2	54322.03628	9.996	0.39	0.4041
2	54342.38356	9.270	0.41	0.0718	2	54322.04291	10.020	0.39	0.4183
2	54342.39431	9.309	0.41	0.1066	2	54322.04787	10.036	0.39	0.4290
2	54342.40291	9.337	0.42	0.1345	2	54322.05285	10.051	0.39	0.4396
2	54342.41148	9.363	0.42	0.1623	2	54322.05709	10.064	0.39	0.4487
2	54342.41535	9.375	0.42	0.1748	3	54348.96281	9.430	0.24	0.1136
2	54342.4233	9.402	0.43	0.2005	3	54348.96887	9.463	0.25	0.1266
2	54342.43593	9.440	0.44	0.2414	3	54348.97549	9.499	0.26	0.1408
3	54394.32964	9.596	0.48	0.3673	3	54348.98044	9.525	0.27	0.1514
3	54394.34037	9.635	0.49	0.4020	3	54348.98544	9.553	0.28	0.1621
3	54394.34896	9.667	0.50	0.4299	3	54348.98968	9.575	0.29	0.1712
3	54394.35756	9.696	0.50	0.4577	4	54395.08432	9.603	0.19	0.9621
3	54394.36141	9.706	0.51	0.4702	4	54395.09038	9.344	0.18	0.9751
3	54394.36936	9.721	0.51	0.4960	4	54395.097	9.105	0.17	0.9893
3	54394.382	9.732	0.52	0.5369	4	54395.10194	9.014	0.16	0.9999
4	54448.08932	9.731	0.52	0.5384	4	54395.10694	8.975	0.16	0.0106
4	54448.09977	9.725	0.53	0.5723	4	54395.11119	8.974	0.16	0.0197
4	54448.1081	9.716	0.53	0.5993	5	54489.86693	9.334	0.22	0.1020
4	54448.11644	9.705	0.53	0.6263	5	54489.87301	9.373	0.23	0.1151
5	54484.14804	9.588	0.47	0.3619	5	54489.87963	9.416	0.25	0.1292
5	54484.1585	9.628	0.49	0.3958	5	54489.88462	9.448	0.26	0.1399
5	54484.16683	9.659	0.49	0.4228	5	54489.88956	9.480	0.26	0.1505
5	54484.17516	9.686	0.50	0.4498	5	54489.89382	9.506	0.27	0.1597
6	54580.05927	9.309	0.41	0.0961	6	54516.76767	10.190	0.39	0.7562
6	54580.06972	9.350	0.42	0.1300	6	54516.77373	10.191	0.39	0.7692
6	54580.07806	9.381	0.42	0.1570	6	54516.78035	10.189	0.38	0.7834
6	54580.08639	9.408	0.42	0.1840	6	54516.78532	10.190	0.37	0.7941
7	54622.23102	9.602	0.51	0.7246	6	54516.79029	10.193	0.36	0.8047
7	54622.24147	9.508	0.50	0.7585	6	54516.79454	10.196	0.36	0.8138
7	54622.2498	9.399	0.49	0.7855	7	54578.98769	9.417	0.22	0.1074
7	54622.25814	9.285	0.47	0.8125	7	54578.99372	9.444	0.23	0.1203
8	54677.10959	9.724	0.52	0.5208	7	54579.00032	9.476	0.25	0.1344
8	54677.12003	9.721	0.52	0.5546	7	54579.00529	9.500	0.26	0.1451
8	54677.12838	9.715	0.53	0.5817	7	54579.01028	9.524	0.27	0.1558
8	54677.1367	9.704	0.53	0.6086	7	54579.01453	9.543	0.27	0.1649
9	54730.0075	9.225	0.43	0.9000	8	54623.24464	9.588	0.21	0.9597
9	54730.01795	9.206	0.42	0.9339	8	54623.25071	9.472	0.19	0.9727
9	54730.02628	9.204	0.41	0.9609	8	54623.25734	9.341	0.18	0.9869
9	54730.03462	9.217	0.40	0.9879	8	54623.26228	9.254	0.17	0.9975
10	54778.54648	9.388	0.42	0.1571	8	54623.26728	9.196	0.17	0.0082
10	54778.55722	9.421	0.43	0.1919	8	54623.27152	9.167	0.16	0.0173
10	54778.56581	9.447	0.43	0.2198	9	54702.39156	10.112	0.41	0.5889
10	54778.5744	9.478	0.44	0.2476	9	54702.3966	10.118	0.41	0.5997
10	54778.57826	9.490	0.44	0.2601	9	54702.40324	10.130	0.42	0.6140
10	54778.58622	9.516	0.45	0.2859	9	54702.40819	10.138	0.42	0.6246
10	54778.59884	9.561	0.46	0.3268	9	54702.41318	10.145	0.42	0.6353
11	54837.09566	9.214	0.46	0.8454	9	54702.41742	10.151	0.42	0.6444
11	54837.10639	9.212	0.44	0.8802	10	54781.03128	9.368	0.23	0.1311
11	54837.11498	9.219	0.43	0.9080	10	54781.03465	9.390	0.24	0.1383
11	54837.12355	9.202	0.42	0.9358	10	54781.03947	9.422	0.25	0.1486
11	54837.12742	9.195	0.41	0.9483	10	54781.04615	9.466	0.26	0.1630
11	54837.13537	9.194	0.41	0.9741	10	54781.05123	9.497	0.27	0.1738
11	54837.1473	9.261	0.40	0.0127	10	54781.05826	9.540	0.28	0.1889
12	54959.36343	9.204	0.41	0.9698	11	54954.92647	10.147	0.37	0.8266
12	54959.37416	9.193	0.40	0.0046	11	54954.92878	10.147	0.36	0.8316
12	54959.38274	9.203	0.41	0.0324	11	54954.93449	10.153	0.35	0.8438
12	54959.39133	9.225	0.41	0.0602	11	54954.94096	10.155	0.34	0.8577
12	54959.3952	9.238	0.41	0.0728	11	54954.94594	10.152	0.33	0.8684
12	54959.40315	9.268	0.41	0.0985	11	54954.9541	10.134	0.31	0.8858

Table 2
(Continued)

Set	MJD	V	$B-V$ [a]	Phase	Set	MJD	V	$B-V$ [a]	Phase
12	54959.41578	9.315	0.42	0.1394	12	54997.46322	9.352	0.19	0.9922
13	55168.48128	9.685	0.51	0.4721	12	54997.46659	9.325	0.19	0.9994
13	55168.492	9.713	0.52	0.5068	12	54997.47241	9.298	0.18	0.0119
13	55168.50059	9.728	0.52	0.5347	12	54997.47797	9.287	0.17	0.0238
13	55168.50918	9.734	0.52	0.5625	12	54997.48304	9.289	0.16	0.0347
13	55168.51304	9.734	0.53	0.5750	12	54997.49095	9.313	0.16	0.0517
13	55168.521	9.729	0.53	0.6008	13	55176.44902	10.127	0.41	0.5980
13	55168.53225	9.712	0.53	0.6372	13	55176.45135	10.126	0.41	0.6031
					13	55176.45705	10.127	0.41	0.6153
					13	55176.46355	10.127	0.41	0.6292
					13	55176.46854	10.128	0.42	0.6399
					13	55176.4763	10.123	0.42	0.6565
					14	55341.16571	10.141	0.41	0.6220
					14	55341.16804	10.142	0.41	0.6270
					14	55341.17571	10.152	0.41	0.6435
					14	55341.18219	10.157	0.42	0.6574
					14	55341.18713	10.158	0.42	0.6680
					14	55341.193	10.162	0.42	0.6805
SU Dra					RR Lyr				
2	54396.06873	10.195	0.38	0.5930	1	49984.25103	7.68	0.38	0.417
2	54396.08065	10.195	0.38	0.6111	1	49984.25581	7.68	0.38	0.425
2	54396.09115	10.191	0.39	0.6263	1	49984.26076	7.69	0.38	0.434
2	54396.0953	10.190	0.39	0.6323	1	49984.26525	7.69	0.38	0.442
3	54426.18972	9.794	0.28	0.2019	1	49984.27176	7.7	0.38	0.453
3	54426.20164	9.826	0.30	0.2201	1	49984.27638	7.71	0.38	0.461
3	54426.21214	9.851	0.31	0.2353	4	50047.04674	7.36	0.30	0.200
3	54426.21628	9.859	0.31	0.2413	4	50047.05186	7.37	0.31	0.209
4	54478.92392	9.472	0.14	0.0514	4	50047.05669	7.39	0.32	0.218
4	54478.93418	9.504	0.15	0.0665	4	50047.0617	7.4	0.32	0.227
4	54478.94468	9.540	0.16	0.0832	4	50047.06661	7.41	0.33	0.235
4	54478.94877	9.554	0.17	0.0892	4	50047.07193	7.43	0.34	0.245
4	54478.95101	9.562	0.17	0.0923	5	50172.97726	7.63	0.39	0.366
4	54478.96269	9.602	0.19	0.1104	5	50172.98699	7.64	0.39	0.383
4	54478.97122	9.626	0.21	0.1225	5	50172.9915	7.65	0.39	0.391
4	54478.97532	9.638	0.21	0.1286	5	50172.99797	7.66	0.38	0.402
5	54492.91603	9.852	0.31	0.2380	5	50173.00264	7.67	0.38	0.411
5	54492.92925	9.886	0.32	0.2576	6	50186.85366	7.91	0.42	0.847
5	54492.94056	9.908	0.33	0.2758	6	50186.85845	7.91	0.41	0.855
5	54492.94468	9.916	0.33	0.2819	6	50186.86339	7.93	0.40	0.864
6	54532.48479	9.701	0.24	0.1530	6	50186.86788	7.93	0.39	0.872
6	54532.49495	9.729	0.25	0.1667	6	50186.87441	7.94	0.37	0.883
6	54532.50539	9.758	0.27	0.1833	6	50186.879	7.95	0.36	0.891
6	54532.50948	9.770	0.27	0.1894	7	50201.05711	7.94	0.34	0.904
6	54532.51167	9.775	0.28	0.1939	7	50201.06191	7.93	0.33	0.913
6	54532.52188	9.804	0.29	0.2106	7	50201.06684	7.93	0.31	0.921
6	54532.53042	9.825	0.30	0.2242	7	50201.07133	7.92	0.30	0.929
6	54532.53456	9.836	0.30	0.2303	7	50201.07787	7.89	0.28	0.941
7	54586.25231	10.199	0.37	0.5666	7	50201.08245	7.86	0.27	0.949
7	54586.26252	10.207	0.38	0.5833	8	50228.80167	7.9	0.42	0.851
7	54586.27297	10.214	0.38	0.5984	8	50228.80661	7.91	0.41	0.860
7	54586.27706	10.212	0.38	0.6045	8	50228.81119	7.92	0.40	0.868
7	54586.27925	10.210	0.38	0.6075	8	50228.81616	7.93	0.38	0.876
7	54586.28946	10.206	0.39	0.6257	8	50228.8208	7.94	0.37	0.885
7	54586.298	10.203	0.39	0.6378	8	50228.82721	7.94	0.35	0.896
7	54586.30214	10.201	0.39	0.6439	9	50562.87498	7.51	0.32	0.220
8	54639.00762	10.096	0.35	0.4494	9	50562.88171	7.52	0.33	0.232
8	54639.01944	10.113	0.35	0.4660	9	50562.88664	7.53	0.34	0.241
8	54639.02994	10.126	0.36	0.4827	9	50562.89113	7.54	0.34	0.249
8	54639.03405	10.130	0.36	0.4887	9	50562.89767	7.55	0.35	0.260
9	54733.1287	9.477	0.20	0.9667	9	50562.90226	7.56	0.36	0.268
9	54733.1406	9.477	0.20	0.9667	10	50567.58263	7.77	0.39	0.525
9	54733.1511	9.388	0.17	0.9849	10	50567.58936	7.77	0.39	0.537
9	54733.15524	9.388	0.17	0.9849	10	50567.59429	7.77	0.40	0.546
10	54833.63013	9.660	0.23	0.1446	10	50567.59878	7.78	0.40	0.554
10	54833.64205	9.697	0.25	0.1627	10	50567.60532	7.78	0.40	0.565

Table 2
(Continued)

Set	MJD	V	$B-V$ [a]	Phase	Set	MJD	V	$B-V$ [a]	Phase
10	54833.65253	9.726	0.26	0.1794	10	50567.60991	7.78	0.41	0.573
10	54833.65667	9.738	0.27	0.1854	11	50745.19083	7.94	0.41	0.860
12	55130.18997	9.761	0.28	0.1935	11	50745.19752	7.95	0.39	0.872
12	55130.19992	9.791	0.29	0.2086	11	50745.20249	7.95	0.38	0.881
12	55130.2095	9.819	0.30	0.2238	11	50745.20698	7.96	0.37	0.889
12	55130.21683	9.837	0.31	0.2344	11	50745.2135	7.95	0.35	0.900
13	55143.86819	10.080	0.28	0.9046	11	50745.2181	7.94	0.33	0.908
13	55143.87203	10.005	0.28	0.9107	12	50749.22225	7.36	0.23	0.972
13	55143.87913	9.831	0.26	0.9213	12	50749.22894	7.26	0.22	0.984
13	55143.88887	9.711	0.24	0.9364	12	50749.2339	7.19	0.21	0.993
13	55143.89302	9.673	0.23	0.9425	12	50749.2384	7.13	0.17	0.001
13	55143.90014	9.585	0.22	0.9531	12	50749.24358	7.09	0.16	0.010
13	55143.90985	9.462	0.19	0.9682	12	50749.24821	7.06	0.15	0.018
13	55143.91834	9.395	0.18	0.9803	13	54781.1015	7.81	0.22	0.978
15	55149.26255	9.522	0.15	0.0737	13	54781.10757	7.73	0.21	0.989
15	55149.2725	9.556	0.17	0.0903	13	54781.11395	7.66	0.20	1.000
15	55149.28207	9.587	0.19	0.1040	13	54781.12127	7.58	0.16	0.013
15	55149.28941	9.610	0.19	0.1130	13	54781.12775	7.51	0.15	0.024
16	55317.09729	9.793	0.29	0.2067	14	54781.16808	7.4	0.17	0.095
16	55317.10911	9.824	0.30	0.2248	14	54781.17414	7.42	0.18	0.106
16	55317.11961	9.850	0.31	0.2415	14	54781.18052	7.44	0.19	0.117
16	55317.12375	9.859	0.31	0.2476	14	54781.18786	7.47	0.21	0.130
					14	54781.19433	7.49	0.22	0.142
					15	54781.36779	7.84	0.38	0.448
					15	54781.37385	7.85	0.38	0.458
					15	54781.38023	7.86	0.38	0.470
					15	54781.38756	7.86	0.38	0.483
					15	54781.39404	7.87	0.38	0.494
					16	54782.10012	7.91	0.48	0.740
					16	54782.10618	7.91	0.48	0.750
					16	54782.11256	7.91	0.48	0.762
					16	54782.11988	7.91	0.48	0.775
					16	54782.12637	7.91	0.47	0.786
					17	54784.16409	7.78	0.39	0.381
					17	54784.17015	7.79	0.39	0.392
					17	54784.17653	7.79	0.38	0.403
					17	54784.18385	7.8	0.38	0.416
					17	54784.19034	7.81	0.38	0.427
UV Oct					VY Pyx				
1	54280.88854	9.663	0.38	0.3749	1	54391.79701	7.284	0.55	0.2171
1	54280.89363	9.677	0.38	0.3889	1	54391.80337	7.290	0.55	0.2223
1	54280.90203	9.696	0.38	0.3983	1	54391.80916	7.289	0.56	0.2269
1	54280.90706	9.708	0.38	0.4138	1	54391.81659	7.293	0.56	0.2329
2	54321.13128	9.695	0.38	0.4231	1	54391.82215	7.296	0.56	0.2374
2	54321.13642	9.697	0.44	0.6712	2	54399.99065	7.227	0.54	0.8252
2	54321.14453	9.704	0.44	0.6806	2	54399.997	7.223	0.54	0.8303
2	54321.1551	9.717	0.44	0.6956	2	54400.00278	7.222	0.54	0.8350
2	54321.16021	9.724	0.44	0.7151	2	54400.01022	7.215	0.53	0.8410
3	54371.95272	9.421	0.44	0.7245	2	54400.01578	7.212	0.53	0.8454
3	54371.95787	9.432	0.30	0.1851	3	54406.38762	7.194	0.51	0.9842
3	54371.96595	9.451	0.31	0.1945	3	54406.39397	7.194	0.51	0.9893
3	54371.97653	9.476	0.32	0.2094	3	54406.39975	7.194	0.50	0.9940
3	54371.98163	9.488	0.33	0.2289	3	54406.40719	7.194	0.50	0.0000
4	54376.00938	9.648	0.34	0.2383	3	54406.41275	7.197	0.50	0.0045
4	54376.01451	9.662	0.44	0.6945	4	54414.18113	7.313	0.57	0.2695
4	54376.0226	9.689	0.44	0.7040	4	54414.18749	7.315	0.57	0.2747
4	54376.03318	9.727	0.44	0.7189	4	54414.19328	7.318	0.57	0.2793
4	54376.0383	9.745	0.43	0.7384	4	54414.20071	7.321	0.57	0.2853
5	54522.69065	9.172	0.43	0.7479	4	54414.20626	7.323	0.57	0.2898
5	54522.69579	9.185	0.16	0.0250	5	54421.04014	7.242	0.55	0.8012
5	54522.70389	9.208	0.16	0.0344	5	54421.04649	7.237	0.54	0.8063
5	54522.71447	9.233	0.17	0.0494	5	54421.05229	7.235	0.54	0.8110
5	54522.71955	9.243	0.19	0.0689	5	54421.05972	7.228	0.54	0.8170
6	54551.36091	9.377	0.20	0.0782	5	54421.06527	7.227	0.54	0.8215
6	54551.36606	9.243	0.34	0.8636	6	54427.69953	7.266	0.54	0.1719

5

Table 2
(Continued)

Set	MJD	V	B − V [a]	Phase	Set	MJD	V	B − V [a]	Phase
6	54551.37417	9.033	0.33	0.8731	6	54427.70588	7.268	0.54	0.1770
6	54551.38473	8.868	0.31	0.8881	6	54427.71167	7.269	0.54	0.1817
6	54551.38984	8.834	0.29	0.9075	6	54427.7191	7.273	0.54	0.1877
7	54569.72058	9.757	0.28	0.9169	6	54427.72465	7.276	0.54	0.1922
7	54569.72574	9.762	0.44	0.7001	7	54439.55301	7.300	0.57	0.7315
7	54569.73384	9.778	0.44	0.7096	7	54439.55938	7.297	0.57	0.7367
7	54569.74442	9.797	0.44	0.7245	7	54439.56516	7.293	0.56	0.7413
7	54569.74951	9.806	0.43	0.7440	7	54439.57259	7.286	0.56	0.7473
8	54601.98409	9.356	0.43	0.7534	7	54439.57815	7.284	0.56	0.7518
8	54601.98925	9.368	0.28	0.1610	8	54458.27282	7.213	0.54	0.8287
8	54601.99733	9.390	0.29	0.1706	8	54458.2792	7.209	0.54	0.8339
8	54602.00791	9.418	0.30	0.1854	8	54458.28498	7.205	0.54	0.8385
8	54602.01302	9.430	0.31	0.2049	8	54458.29241	7.202	0.53	0.8445
9	54660.78087	9.629	0.32	0.2144	8	54458.29796	7.200	0.53	0.8490
9	54660.78602	9.629	0.40	0.5222	9	54466.59728	7.424	0.60	0.5423
9	54660.79411	9.630	0.40	0.5317	9	54466.60366	7.423	0.60	0.5474
9	54660.80468	9.635	0.41	0.5466	9	54466.60944	7.424	0.60	0.5521
9	54660.80979	9.639	0.41	0.5661	9	54466.61686	7.423	0.60	0.5581
10	54704.02235	9.446	0.42	0.5755	9	54466.62242	7.421	0.60	0.5625
10	54704.02749	9.458	0.32	0.2153	10	54471.59201	7.416	0.60	0.5704
10	54704.03559	9.479	0.33	0.2248	10	54471.59838	7.413	0.60	0.5756
10	54704.04617	9.508	0.34	0.2397	10	54471.60417	7.413	0.60	0.5802
10	54704.05126	9.523	0.35	0.2592	10	54471.6116	7.410	0.60	0.5862
11	54900.0444	9.714	0.35	0.2686	10	54471.61716	7.408	0.60	0.5907
11	54900.04955	9.717	0.39	0.4797	11	54482.71326	7.412	0.60	0.5395
11	54900.05764	9.719	0.39	0.4892	11	54482.71963	7.412	0.60	0.5447
11	54900.06822	9.724	0.40	0.5041	11	54482.72542	7.411	0.60	0.5493
11	54900.07331	9.727	0.40	0.5236	11	54482.73285	7.411	0.60	0.5553
12	54908.69757	9.660	0.40	0.5330	11	54482.7384	7.406	0.60	0.5598
12	54908.70125	9.662	0.38	0.4273	12	54491.30479	7.406	0.60	0.4685
12	54908.70933	9.668	0.38	0.4341	12	54491.31115	7.405	0.60	0.4736
12	54908.71991	9.670	0.39	0.4490	12	54491.31693	7.408	0.61	0.4782
12	54908.725	9.671	0.39	0.4685	12	54491.32436	7.409	0.61	0.4842
13	55075.29118	9.626	0.39	0.4779	12	54491.32993	7.411	0.61	0.4887
13	55075.29632	9.628	0.39	0.4557	13	54499.62819	7.271	0.54	0.1811
13	55075.30442	9.631	0.39	0.4652	13	54499.63456	7.272	0.54	0.1863
13	55075.315	9.637	0.39	0.4801	13	54499.64035	7.273	0.54	0.1909
13	55075.32008	9.640	0.40	0.4996	13	54499.64778	7.275	0.55	0.1969
14	55087.85755	9.681	0.40	0.5090	13	54499.65333	7.277	0.55	0.2014
14	55087.86269	9.682	0.43	0.6153	14	54526.47303	7.217	0.54	0.8310
14	55087.87078	9.696	0.43	0.6247	14	54526.47941	7.215	0.54	0.8362
14	55087.88135	9.725	0.43	0.6396	14	54526.48519	7.212	0.53	0.8408
14	55087.88646	9.740	0.44	0.6591	14	54526.49262	7.208	0.53	0.8468
15	55148.83507	9.040	0.44	0.6685	14	54526.49818	7.207	0.53	0.8513
15	55148.84021	9.066	0.18	0.9955	15	54532.39944	7.395	0.60	0.6106
15	55148.8483	9.110	0.15	0.0050	15	54532.40581	7.392	0.59	0.6157
15	55148.85888	9.161	0.16	0.0199	15	54532.4116	7.384	0.59	0.6204
15	55148.86398	9.183	0.17	0.0394	15	54532.41903	7.381	0.59	0.6264
					15	54532.42458	7.380	0.59	0.6309
					16	54799.06059	7.353	0.58	0.6682
					16	54799.06696	7.351	0.58	0.6733
					16	54799.07274	7.347	0.58	0.6780
					16	54799.08017	7.340	0.58	0.6840
					16	54799.08573	7.338	0.58	0.6885
					17	54817.77185	7.279	0.56	0.7585
					17	54817.77822	7.272	0.56	0.7636
					17	54817.784	7.268	0.56	0.7683
					17	54817.79144	7.265	0.55	0.7743
					17	54817.79699	7.260	0.55	0.7788
					18	54860.52883	7.285	0.56	0.2413
					18	54860.53521	7.287	0.56	0.2464
					18	54860.541	7.292	0.56	0.2511
					18	54860.54843	7.297	0.56	0.2571
					18	54860.55398	7.298	0.57	0.2616
					19	55289.58789	7.310	0.57	0.2700

Table 2
(Continued)

Set	MJD	V	B − V [a]	Phase	Set	MJD	V	B − V [a]	Phase
					19	55289.59426	7.309	0.57	0.2752
					19	55289.60003	7.314	0.57	0.2798
					19	55289.60747	7.318	0.57	0.2858
					19	55289.61303	7.318	0.57	0.2903
					20	55301.43772	7.222	0.54	0.8267
					20	55301.44407	7.218	0.54	0.8318
					20	55301.44985	7.215	0.54	0.8365
					20	55301.45728	7.211	0.53	0.8425
					20	55301.46285	7.207	0.53	0.8470
					21	55325.93291	7.409	0.60	0.5816
					21	55325.93927	7.408	0.60	0.5868
					21	55325.94506	7.406	0.60	0.5914
					21	55325.95249	7.404	0.60	0.5974
					21	55325.95804	7.403	0.60	0.6019
					22	55332.25647	7.344	0.58	0.6815
					22	55332.26284	7.341	0.58	0.6866
					22	55332.26862	7.339	0.58	0.6913
					22	55332.27605	7.334	0.58	0.6973
					22	55332.28161	7.331	0.58	0.7018
					23	55351.36845	7.227	0.52	0.0950
					23	55351.37481	7.229	0.52	0.1001
					23	55351.3806	7.230	0.52	0.1048
					23	55351.38803	7.231	0.52	0.1108
					23	55351.39359	7.234	0.52	0.1152
κ Pav									
1	54280.81179	4.207	0.60	0.1921					
1	54280.82106	4.210	0.61	0.1931					
1	54280.82566	4.212	0.61	0.1936					
1	54280.83559	4.212	0.61	0.1947					
2	54321.05596	4.633	0.86	0.6235					
2	54321.06751	4.634	0.86	0.6248					
2	54321.07611	4.631	0.86	0.6258					
2	54321.08404	4.633	0.86	0.6266					
2	54321.09235	4.633	0.86	0.6276					
2	54321.10119	4.631	0.86	0.6285					
3	54373.07462	4.472	0.82	0.3516					
3	54373.08557	4.474	0.82	0.3528					
3	54373.09296	4.475	0.83	0.3536					
3	54373.1042	4.477	0.83	0.3548					
3	54373.11263	4.480	0.83	0.3558					
3	54373.12443	4.482	0.83	0.3571					
4	54519.03565	4.569	0.89	0.4241					
4	54519.04564	4.571	0.89	0.4252					
4	54519.05097	4.572	0.89	0.4258					
4	54519.06171	4.575	0.89	0.4270					
5	54548.08718	4.662	0.86	0.6231					
5	54548.09788	4.660	0.86	0.6243					
5	54548.10277	4.659	0.86	0.6248					
5	54548.11111	4.660	0.86	0.6258					
5	54548.11814	4.660	0.86	0.6265					
5	54548.12516	4.657	0.86	0.6273					
7	54601.02693	4.613	0.90	0.4526					
7	54601.03856	4.614	0.90	0.4539					
7	54601.04464	4.613	0.90	0.4545					
7	54601.05392	4.612	0.90	0.4556					
7	54601.06093	4.612	0.90	0.4563					
7	54601.06792	4.617	0.90	0.4571					
8	54653.05113	4.192	0.59	0.1813					
8	54653.06206	4.196	0.59	0.1825					
8	54653.06906	4.196	0.59	0.1832					
8	54653.0803	4.196	0.59	0.1845					
8	54653.08878	4.201	0.59	0.1854					
8	54653.10058	4.203	0.60	0.1867					
9	54659.04949	4.219	0.57	0.8418					
9	54659.06061	4.215	0.57	0.8430					

7

Table 2
(Continued)

Set	MJD	V	$B - V$ [a]	Phase	Set	MJD	V	$B - V$ [a]	Phase
9	54659.06693	4.211	0.57	0.8437					
9	54659.07627	4.205	0.57	0.8447					
10	54705.88251	3.965	0.42	0.9988					
10	54705.89347	3.963	0.42	1.0000					
10	54705.9005	3.963	0.42	0.0008					
10	54705.9117	3.963	0.42	0.0020					
10	54705.92017	3.963	0.42	0.0029					
10	54705.93197	3.961	0.42	0.0042					
12	54877.21429	4.102	0.54	0.8650					
12	54877.22524	4.097	0.54	0.8662					
12	54877.23265	4.094	0.54	0.8670					
12	54877.24388	4.089	0.54	0.8683					
12	54877.25233	4.083	0.54	0.8692					
12	54877.26414	4.078	0.53	0.8705					
13	54986.28763	4.078	0.53	0.8757					
13	54986.30008	4.074	0.52	0.8770					
13	54986.30903	4.069	0.52	0.8780					
13	54986.32178	4.064	0.52	0.8794					
13	54986.33166	4.064	0.52	0.8805					
13	54986.34207	4.061	0.52	0.8816					
14	55093.89644	4.596	0.75	0.7250					
14	55093.90741	4.596	0.74	0.7262					
14	55093.91481	4.596	0.74	0.7270					
14	55093.92604	4.594	0.74	0.7283					
14	55093.93447	4.593	0.74	0.7292					
14	55093.94627	4.594	0.74	0.7305					
15	55148.88147	4.531	0.67	0.7797					
15	55148.8887	4.529	0.67	0.7805					
15	55148.89303	4.527	0.66	0.7810					
15	55148.89762	4.524	0.66	0.7815					
15	55148.90877	4.523	0.66	0.7827					
15	55148.9153	4.523	0.66	0.7834					
15	55148.92083	4.522	0.66	0.7840					
15	55148.92597	4.521	0.66	0.7846					

Note. [a] $B - V$ estimated from phased light curve.
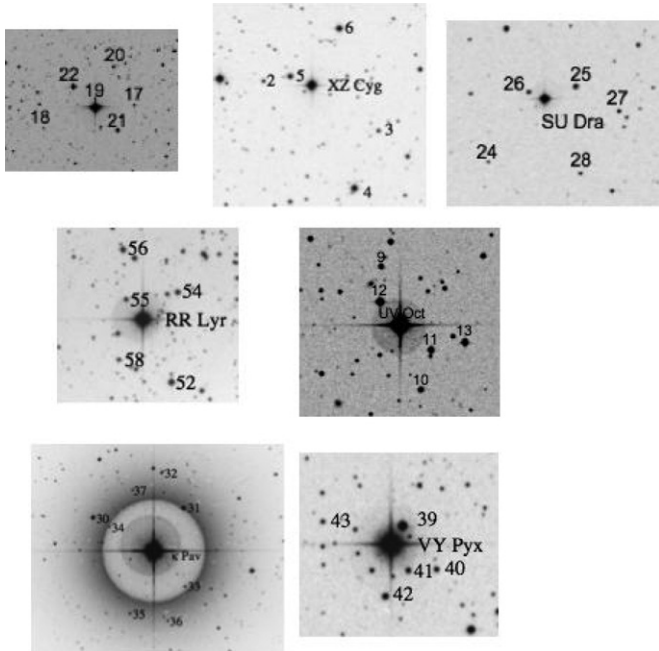
Figure 1. RRL and CP2 fields with astrometric reference stars marked. Boxes are roughly 2′ across with north to the top and east to the left. RZ Cep is at top left.

period, $\langle V \rangle$, $\langle K \rangle$, $\langle B - V \rangle$, $E(B - V)$, A_V, and A_K. Photometry is from the various sources noted in the table. The $\langle K \rangle$ is in the 2MASS system. All reddening values are adopted from those listed in Fernley et al. (1998a) or Feast et al. (2008) with a sanity check provided by our reference star photometry.

Our default metallicity source is Fernley et al. (1998a). The metallicity of RR Lyr is from Kolenberg et al. (2010). The metallicities of UV Oct and VY Pyx were determined for this paper, using the approach described in Kolenberg et al. (2010), determined by an analysis of Fe line equivalent widths measured from high-resolution spectra. The κ Pav metallicity is from Luck & Bond (1989). The Fernley et al. (1998a) metallicities agree with Layden (1994) for the brighter stars in common ($V < 11$). Because the Layden (1994) metallicities are on the ZW (Zinn & West 1984) scale, we assume the same scale for the Fernley et al. (1998a) metallicities. Because the Kolenberg et al. (2010) RR Lyrae metallicity agrees with Fernley et al. (1998a), we presume that it too is ZW. Therefore we believe our metallicities are on, or close to, the ZW scale. This is the scale we use to establish zero points that will be applied later to derive distances.

Finally, three stars in our sample (including RR Lyrae) exhibit Blazhko cycles, wherein the maximum and minimum brightness vary over time. Smith and Kolenberg have studied this phenomenon for many such stars (see, e.g., LaCluyzé et al. 2004; Kolenberg et al. 2006, 2010; Blazhko Project Web

site http://www.univie.ac.at/tops/blazhko/) and conclude from recent data that the total output of the target Blazhko stars averaged over a cycle remains constant within 0.03 mag, in accordance with the findings by Alcock et al. (2003). As the peak brightness decreases, the minimum brightness increases. Blazhko is not a disease that renders RRL poor standard candles as further demonstrated in Cacciari et al. (2005).

3. SPECTROPHOTOMETRIC PARALLAXES OF THE ASTROMETRIC REFERENCE STARS

The following review of our astrometric and spectrophotometric techniques uses the κ Pav field as an example. Because the parallaxes determined for the variables will be measured with respect to reference frame stars which have their own parallaxes, we must either apply a statistically derived correction from relative to absolute parallax (Van Altena et al. 1995, hereafter YPC95) or estimate the absolute parallaxes of the reference frame stars. In principle, the colors, spectral type, and luminosity class of a star can be used to estimate the absolute magnitude, M_V, and V-band absorption, A_V. The absolute parallax is then simply

$$\pi_{\mathrm{abs}} = 10^{\frac{-(V - M_V + 5 - A_V)}{5}}. \qquad (1)$$

The luminosity class is generally more difficult to estimate than the spectral type (temperature class). However, the derived absolute magnitudes are critically dependent on the luminosity class. As a consequence we use as much additional information as possible in an attempt to confirm the luminosity classes. Specifically, we obtain 2MASS[18] photometry and proper motions from the PPMXL catalog (Roeser et al. 2010) for a one degree square field centered on each science target, and iteratively employ the technique of reduced proper motion (Yong & Lambert 2003; Gould & Morgan 2003) to confirm our giant/dwarf classifications (Section 4.2).

3.1. Reference Star Photometry

Our bandpasses for reference star photometry include: BV from recent measurements with the New Mexico State University 1 m telescope (Holtzman et al. 2010) for RR Lyr, SU Dra, XZ Cyg, and RZ Cep fields; from the South African Astronomical Observatory (SAAO) 1 m for the UV Oct, κ Pav, and VY Pyx fields; from the SMARTS 0.9 m (Subasavage et al. 2010) for the VY Pyx and UV Oct fields; and JHK (from 2MASS). Table 3 lists BVJHK photometry for our reference stars bright enough to have 2MASS measurements.

3.2. Reference Star Spectroscopy

Spectral classifications for reference stars in the UV Oct, κ Pav, and VY Pyx fields were provided by the SAAO 1.9 m telescope. The SAAO resolution was 3.5 Å/(FWHM) with wavelength coverage from 3750 Å $\leqslant \lambda \leqslant$ 5500 Å. Spectroscopic classification of the reference stars in the fields of RR Lyr, SU Dra, XZ Cyg, and RZ Cep was accomplished using data obtained with the Double Imaging Spectrograph (DIS) on the Apache Point Observatory 3.5 m telescope.[19] We used the high-resolution gratings, delivering a dispersion of 0.62 Å pixel^{-1},

---

[18] The Two Micron All Sky Survey is a joint project of the University of Massachusetts and the Infrared Processing and Analysis Center/California Institute of Technology.
[19] The Apache Point Observatory 3.5 m telescope is owned and operated by the Astrophysical Research Consortium.

Table 3
Reference Stars: Visible and Near-IR Photometry

FGS ID	PPMXL ID	V	$B - V$	K^a	$J - K$	$V - K$
XZ Cyg						
2	178627907000819000	15.24	0.79 ± 0.11	13.34	0.45	1.90
3	178627806678871000	15.00	0.72 ± 0.1	13.30	0.37	1.70
4	178627507943789000	12.55	1.26 ± 0.03	9.51	0.84	3.04
5	178626897495064000	13.16	0.50 ± 0.04	11.96	0.30	1.20
6	178627902818755000	12.46	0.65 ± 0.03	11.03	0.37	1.43
UV Oct						
9	6050827457780530000	15.92	0.68 ± 0.04	14.25	0.41	1.67
10	6050827543215700000	15.35	0.94 ± 0.05	13.01	0.57	2.35
11	6050827517824970000	14.91	0.63 ± 0.04	13.24	0.40	1.67
12	6050827495380950000	13.12	1.35 ± 0.03	9.82	0.87	3.30
13	6050827141173300000	14.45	0.63 ± 0.04	12.74	0.38	1.71
RZ Cep						
17	236149611067714000	14.90	1.09 ± 0.07	12.26	0.56	2.64
18	236150055842444000	16.30	1.29 ± 0.15	13.04	0.60	3.26
19	236150360634453000	16.16	0.96 ± 0.15	13.32	0.75	2.84
20	236150404085559000	15.31	1.25 ± 0.1	12.52	0.69	2.79
21	236149242851448000	14.06	1.00 ± 0.06	11.74	0.50	2.32
22	236150379961202000	12.52	0.62 ± 0.03	11.01	0.29	1.51
SU Dra						
24	910626741647084000	16.26	0.70 ± 0.12	14.51	0.39	1.76
25	910625310986521000	13.10	0.47 ± 0.04	11.80	0.32	1.30
26	910625114428228000	14.60	1.17 ± 0.06	12.14	0.59	2.46
27	910626124371472000	14.36	0.64 ± 0.05	12.66	0.41	1.70
28	910627013779397000	15.19	0.54 ± 0.09	13.75	0.36	1.44
κ Pav						
31	6417195936484110000	12.65	1.17 ± 0.03	9.98	0.68	2.67
32	6417195914995010000	14.24	0.70 ± 0.05	12.56	0.42	1.68
33	6417196838800320000	14.55	0.93 ± 0.04	12.39	0.49	2.17
34	6417197688468440000	15.94	0.95 ± 0.06	13.72	0.51	2.22
35	6417383894358280000	14.84	0.85 ± 0.04	12.96	0.48	1.88
36	6417383768816120000	15.31	0.88 ± 0.05	13.30	0.53	2.01
37	6417197455800920000	15.7	0.89 ± 0.1	13.74	0.45	1.96
VY Pyx						
39	1264343482^b	12.45	1.34 ± 0.03	9.08	0.89	3.37
40	2735010192495240000	15.31	0.55 ± 0.09	13.77	0.32	1.54
41	1264343537^b	15.30	0.93 ± 0.09	13.08	0.53	2.22
42	2735033696661810000	14.41	0.62 ± 0.05	12.71	0.39	1.70
43	2735057261695820000	16.15	0.52 ± 0.15	14.66	0.29	1.49

Notes.
^{a} J, K from 2MASS catalog.
^{b} ID from 2MASS catalog.

and covering the wavelength range of 3864 Å $\leqslant \lambda \leqslant$ 5158 Å. Spectroscopy of the reference stars in the fields of UV Oct, κ Pav, and VY Pyx was also obtained using the RC Spectrograph on the CTIO Blanco 4 m. The Loral3K CCD detector with KPGL1-1 grating was used to deliver a dispersion of 1.0 Å pixel^{-1}, covering the wavelength range 3500 Å $\leqslant \lambda \leqslant$ 5830 Å. Classifications used a combination of template matching and line ratios. Spectral types for the stars are generally better than ±2 subclasses.

3.3. Interstellar Extinction

To determine interstellar extinction we first plot the reference stars on a $J - K$ versus $V - K$ color–color diagram. A comparison of the relationships between spectral type and intrinsic color against those we measured provides an estimate of reddening. Figure 2 contains the κ Pav $J - K$ versus $V - K$ color–color diagram and reddening vector for $A_V = 1.0$. Also plotted are mappings between spectral type and luminosity class V and III from Bessell & Brett (1988) and Cox (2000). Figure 2, along
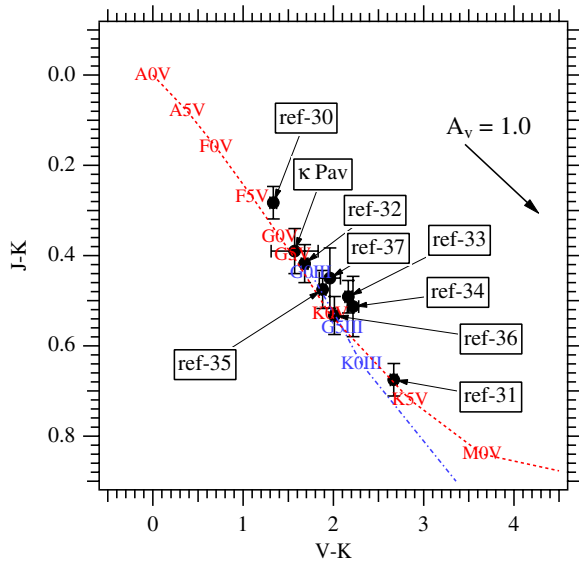
Figure 2. $J - K$ vs. $V - K$ color–color diagram for κ Pav and reference stars. The dashed line is the locus of dwarf (luminosity class V) stars of various spectral types; the dot-dashed line is for giants (luminosity class III). The reddening vector indicates $A_V = 1.0$ for the plotted color systems. For this field at Galactic latitude $\ell^{II} = -25°$, $\langle A_V \rangle = 0.05 \pm 0.06$ mag (Table 4) with a maximum of 0.22 (Schlegel et al. 1998).

(A color version of this figure is available in the online journal.)

with the estimated spectral types, provides an indication of the reddening for each reference star.

Assuming an $R = 3.1$ Galactic reddening law (Savage & Mathis 1979), we derive A_V values by comparing the measured colors (Table 3) with intrinsic $(V - K)_0$ and $(B - V)_0$ colors from Cox (2000). We estimate A_V from $A_V = 1.1E(V - K) = 3.1E(B - V)$, where the ratios of total to selective extinction were derived from the Savage & Mathis (1979) reddening law and a reddening estimate in the direction of κ Pav from Schlegel et al. (1998), via NED.[20] All resulting A_V are collected in Table 4. These are the A_V used in Equation (1).

Using the κ Pav field as an example, we find that the technique of reduced proper motions can provide a possible confirmation of reference star estimated luminosity classes. The precision of existing proper motions for all the reference stars is ~5 mas yr^{-1}, only suggesting discrimination between giants and dwarfs. Typical errors on H_K, a parameter equivalent to absolute magnitude, M, were about a magnitude. Nonetheless, a reduced proper-motion diagram did suggest that ref-31 is not a dwarf star. Our luminosity class uncertainty is reflected in the input spectrophotometric parallax errors (Table 4). We will revisit this additional test in Section 4.2, once we have higher precision proper motions obtained from our modeling.

3.4. Estimated Reference Frame Absolute Parallaxes

We derive absolute parallaxes for each reference star using M_V values as a function of spectral type and luminosity class from Cox (2000) and the A_V derived from the photometry. Our adopted errors for $(m - M)_0$ are 0.5 mag for all reference stars. This error includes uncertainties in A_V and the spectral types used to estimate M_V. Our reference star parallax estimations from Equation (1) are listed in Table 4. Similar data for the RR Lyr reference frame can be found in Benedict et al. (2002b). For the κ Pav field individually, no reference star absolute

---

Table 4
Astrometric Reference Star Spectrophotometric Parallaxes

ID	V	Sp. T.	M_V	A_V	$m - M$	π_{abs} (mas)
XZ Cyg						
2	15.24	K0V	5.9	0.0	9.34 $\pm$ 0.5	1.3 $\pm$ 0.3
3	15	G1.5V	4.6	0.3	10.39 0.5	1.0 0.2
4	12.55	K2III	0.5	0.3	12.05 0.5	0.5 0.1
5	13.16	F7V	3.9	0.0	9.3 0.5	1.4 0.3
6	12.46	G2V	4.7	0.0	7.78 0.5	2.8 0.6
UV Oct						
9	15.92	G5V	5.1	0.1	10.8 0.5	0.7 0.2
10	15.35	K0V	5.9	0.4	9.5 0.5	1.6 0.4
11	14.91	G0V	4.2	0.2	10.7 0.5	0.8 0.2
12	13.12	K3III	0.3	0.3	12.8 0.5	0.3 0.1
13	14.45	F9V	4.2	0.2	10.2 0.5	1.0 0.2
RZ Cep						
17	14.9	G1V	4.5	1.4	10.36 0.5	1.6 0.4
18	16.3	G1V	4.5	2.1	11.76 0.5	1.2 0.3
19	16.16	G2V	4.7	1.3	11.48 0.5	0.9 0.2
20	15.31	K0V	5.9	1.1	9.41 0.5	2.2 0.5
21	14.06	G1V	4.5	1.1	9.52 0.5	2.1 0.5
22	12.52	A1V	0.9	1.7	11.61 0.5	1.1 0.2
SU Dra						
24	16.26	G5V	5.1	0.1	11.16 0.5	0.6 0.1
25	13.1	F6V	3.7	0.1	9.42 0.5	1.4 0.3
26	14.6	K2.5V	6.6	0.4	7.97 0.5	3.0 0.7
27	14.36	G5V	5.1	0.0	9.26 0.5	1.4 0.3
28	15.19	F9V	4.2	0.0	10.97 0.5	0.7 0.1
κ Pav						
31	12.65	K1.5III	0.6	0.1	12.1 0.5	0.4 0.1
32	14.24	G3V	4.8	0.2	9.4 0.5	1.4 0.3
33	14.55	K1V	6.2	0.1	8.4 0.5	2.2 0.5
34	15.94	K1V	6.2	0.2	9.8 0.5	1.2 0.3
35	14.84	K0V	5.9	0.0	8.9 0.5	1.6 0.4
36	15.31	K0V	5.9	0.1	9.4 0.5	1.4 0.3
37	15.7	K0V	5.9	0.1	9.8 1.0	1.2 0.5
VY Pyx						
39	12.45	K3III	0.3	0.3	12.15 0.5	0.4 0.1
40	15.31	F4V	3.3	0.5	11.97 0.5	0.5 0.1
41	15.30	G8V	5.6	0.5	9.72 0.5	1.4 0.3
42	14.41	F6V	3.7	0.5	10.73 0.5	0.9 0.2
43	16.15	F4V	3.3	0.4	12.81 0.5	0.3 0.1

parallax is better determined than $\frac{\sigma_\pi}{\pi} = 23\%$. The average absolute parallax for the reference frame is $\langle \pi_{abs} \rangle = 1.5$ mas. We compare this to the correction to absolute parallax discussed and presented in YPC95. Entering YPC95, Section 3.2, Figure 2, with the κ Pav Galactic latitude, $\ell = -25°$, and average magnitude for the reference frame, $\langle V_{ref} \rangle = 14.2$, we obtain a correction to absolute of 1.2 mas. This gives us confidence in our spectrophotometric determination of the correction to absolute parallax. As in past investigations, we prefer to introduce into our reduction model our spectrophotometrically estimated reference star parallaxes as observations with error. The use of spectrophotometric parallaxes offers a more direct (less Galaxy model-dependent) way of determining the reference star absolute parallaxes.

4. ABSOLUTE PARALLAXES OF POPULATION II VARIABLE STARS

4.1. The Astrometric Model

With the positions measured by FGS 1r (and FGS 3 for RR Lyr) we determine the scale, rotation, and offset "plate

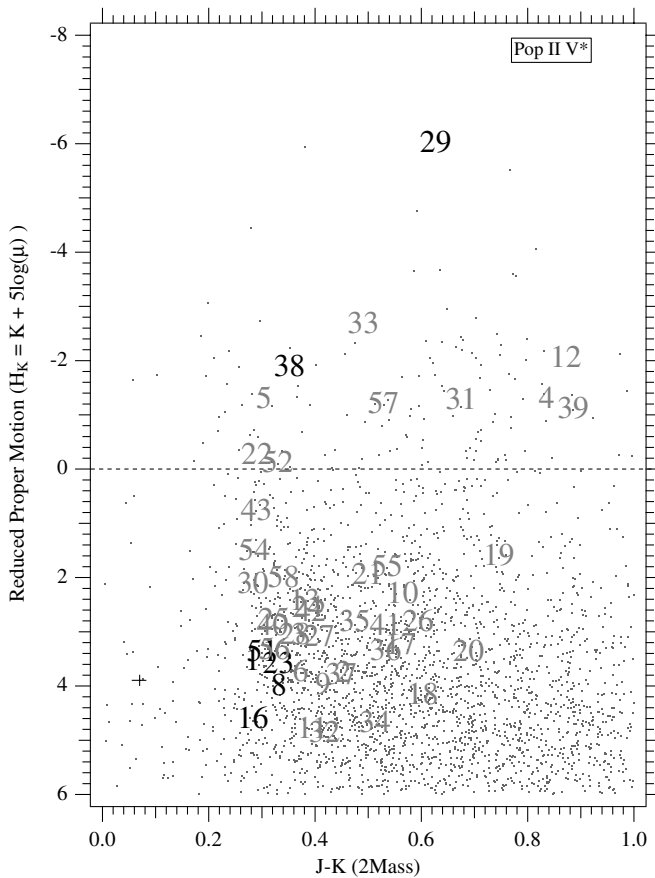**Figure 3.** Reduced proper-motion diagram for 4039 stars taken from $\frac{1}{3}° \times \frac{1}{3}°$ fields centered on each variable star. Star identifications are shown (black) for XZ Cyg (1), UV Oct (8), RZ Cep (16), SU Dra (23), κ Pav (29), VY Pyx (38), RR Lyr (51), and for (gray) all astrometric reference stars in Table 4. Ref-52 through ref-58 are from Benedict et al. (2002b). H_K for all numbered stars is calculated using our final proper motions, examples of which for the κ Pav field can be found in Table 5. For a given spectral type, giants and subgiants have more negative H_K values and are redder than dwarfs in $J - K$. Reference stars ref-4, ref-12, ref-31, and ref-39 are confirmed giants. The plotted position (but not the colors from Table 3) suggests a subgiant classification for ref-33. The cross in the lower left corner indicates representative internal errors along each axis.

Table 5
κ Pav and Reference Star Relative Proper Motion, Parallax, and Space Velocity

ID	μ_x[a]	μ_y[a]	π_{abs}[b]	V_t[c]
κ Pav[d]	-7.41 ± 0.24	16.41 ± 0.24	5.57 ± 0.28	15.3 ± 0.9
31	3.38 ± 0.23	-4.79 ± 0.22	1.82 ± 0.25	15.2 ± 2.5
32	29.47 ± 0.73	-0.26 ± 0.97	1.16 ± 0.42	120.9 ± 443.4
33	0.89 ± 0.33	-0.28 ± 0.35	0.17 ± 0.27	25.2 ± 51.5
34	-0.11 ± 0.50	-15.51 ± 0.44	0.26 ± 0.42	280 ± 1311
35	-8.80 ± 1.15	-3.04 ± 1.03	1.74 ± 0.42	25.4 ± 11.1
36	-9.79 ± 0.39	-3.55 ± 0.42	1.15 ± 0.34	42.8 ± 13.7
37	9.80 ± 0.49	-3.31 ± 0.44	1.46 ± 0.33	33.5 ± 8.9

Notes.
[a] μ_x and μ_y are relative motions along R.A. and decl. in mas yr^{-1}.
[b] Parallax in mas.
[c] $V_t = 4.74 \times \mu/\pi_{abs}$.
[d] Modeled with Equations (2)–(5).

where x and y are the measured coordinates from *HST*; lc_x and lc_y are the lateral color corrections; ΔXFx and ΔXFy are the cross-filter corrections in x and y, applied only to the observations of RR Lyr and the CP2; and $B - V$ are the $B - V$ colors of each star. A and B are scale and rotation plate constants, C and F are offsets; μ_x and μ_y are proper motions; Δt is the epoch difference from the mean epoch; P_α and P_δ are parallax factors; and π_x and π_y are the parallaxes in x and y. We obtain the parallax factors from a JPL Earth orbit predictor (Standish 1990), upgraded to version DE405.

4.2. Prior Knowledge and Modeling Constraints

In a quasi-Bayesian approach the reference star spectrophotometric absolute parallaxes (Table 4) and PPMXL proper motions (Table 5) were input as observations with associated errors, not as hardwired quantities known to infinite precision. Input proper-motion values have typical errors of 4–6 mas yr^{-1} for each coordinate. The lateral color and cross-filter calibrations and the $B - V$ color indices are also treated as observations with error. Proper-motion values obtained from our modeling of *HST* data for the κ Pav field are listed in Table 5. Transverse velocities for κ Pav and all our other science targets, given our final parallaxes, are listed below. We employ the technique of reduced proper motions to provide a confirmation of all reference star estimated luminosity classes listed in Table 4. We obtain proper motion and J, K photometry from PPMXL and 2MASS for a $\frac{1}{3}° \times \frac{1}{3}°$ field centered on all RRL and CP2. Figure 3 shows $H_K = K + 5\log(\mu)$ plotted against $J - K$ color index for 4039 stars. If all stars had the same transverse velocities, Figure 3 would be equivalent to an H-R diagram. The RRL, CP2, and associated reference stars are plotted as ID numbers from Table 5. With our now measured, more precise proper motion (Table 5) errors in H_K are now ∼0.3 mag. Note the clumping of the RRL toward the "faint" end of the diagram. Reduced proper-motion diagrams are "fooled" by the relatively high space velocities of these halo component giant stars.

We stress that for no CP2 or RRL in our program was a previously measured parallax used as prior knowledge and entered as an observation with error. Only reference star parallax prior knowledge was so employed. Our parallax results are blind to previous RRL and CP2 parallax measures from *Hipparcos* and/or parallaxes from surface brightness estimates.

4.3. Assessing Reference Frame Residuals

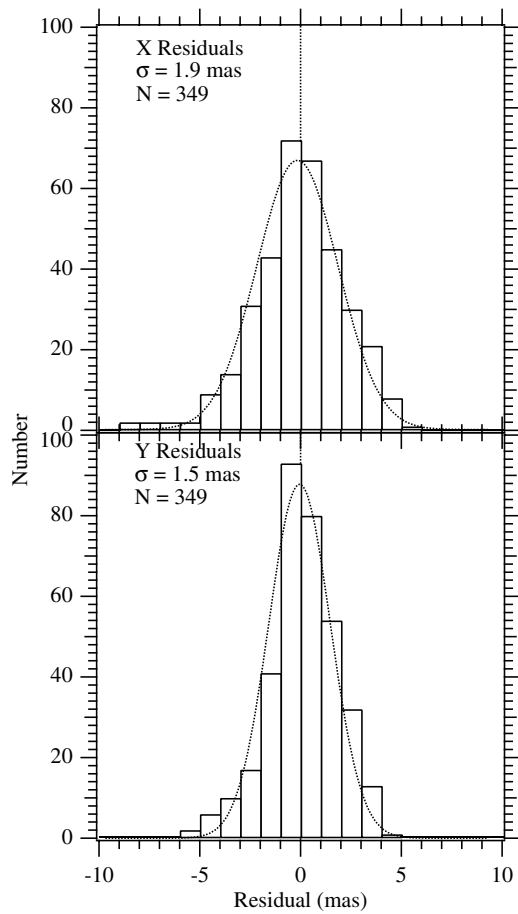The Optical Field Angle Distortion calibration (McArthur et al. 2002) reduces as-built *HST* telescope and FGS 1r

constants" relative to an arbitrarily adopted constraint epoch (the so-called "master plate") for each observation set (the data acquired at each epoch). The MJD of each observation set is listed in Table 2, along with a measured magnitude transformed from the FGS instrumental system as per Benedict et al. (1998), but with coefficients determined for FGS 1r. Our κ Pav reference frame contains six stars. Several primary science targets (RR Lyr, VY Pyx, and κ Pav) are bright enough to require the use of the FGS neutral density filter. For those objects we use the modeling approach outlined in Benedict et al. (2002b), with corrections for both cross-filter and lateral color positional shifts, using values specific to FGS 1r or FGS 3 determined from previous calibration observations with each FGS.

We employ GaussFit (Jefferys et al. 1988) to minimize χ^2. The solved equations of condition for the κ Pav field are

$$x' = x + lc_x (B - V) - \Delta XFx \tag{2}$$

$$y' = y + lc_y (B - V) - \Delta XFy \tag{3}$$

$$\xi = Ax' + By' + C - \mu_x \Delta t - P_\alpha \pi_x \tag{4}$$

$$\eta = -Bx' + Ay' + F - \mu_y \Delta t - P_\delta \pi_y \tag{5}$$

Figure 4. Histograms of *x* and *y* residuals obtained from modeling κ Pav and astrometric reference stars with Equations (4) and (5), constraining $D = -B$ and $E = A$. Distributions are fit with Gaussians whose 1σ dispersions are noted in the plots.

Table 6
κ Pav and Reference Star Relative Positions[a]

FGS ID	V	ξ[b]	η[b]
κ Pav	4.23	-57.7608 ± 0.0002	-156.2033 ± 0.0002
31	12.65	-75.1709 ± 0.0010	-47.2432 ± 0.0012
32[c]	14.23	0.0000 ± 0.0003	0.0000 ± 0.0003
33	14.53	-150.7073 ± 0.0003	-195.2863 ± 0.0003
34	15.81	48.7661 ± 0.0007	-151.6338 ± 0.0010
35	14.84	-70.5595 ± 0.0004	-298.9709 ± 0.0004
36	15.3	-149.3689 ± 0.0003	-278.0559 ± 0.0003
37	15.68	38.8649 ± 0.0004	-59.3234 ± 0.0005

Notes.
[a] Epoch 2007.744.
[b] ξ and η are relative positions in arcseconds.
[c] R.A. = 284°.230996, decl. = -67°.187251, J2000, epoch 2007.744.

distortions with amplitude $\sim 1''$ to below 2 mas over much of the FGS 1r field of regard. From histograms of the κ Pav field astrometric residuals (Figure 4), we conclude that we have obtained satisfactory correction. The resulting reference frame "catalog" in ξ and η standard coordinates (Table 6) was determined with average position errors $\langle \sigma_\xi \rangle = 0.46$ and $\langle \sigma_\eta \rangle = 0.46$ mas.

To determine whether there might be unmodeled—but possibly correctable—systematic effects at the 1 mas level, we plotted reference frame *X* and *Y* residuals against a number of spacecraft, instrumental, and astronomical parameters. These

Table 7
CP2 Parallaxes, Proper Motions, and Absolute Magnitudes

Parameter	κ Pav	VY Pyx
Duration (yr)	2.23	2.63
Ref stars	7	5
Ref $\langle V \rangle$	14.75	14.72
Ref $\langle B - V \rangle$	0.91	0.79
$HST \, \mu$ (mas yr^{-1})	18.1 ± 0.1	31.8 ± 0.2
P.A. (°)	335.5 ± 0.1	20.5 ± 0.1
V_t[a] (km s^{-1})	16.0 ± 0.7	23.4 ± 0.6
$HST \, \pi_{abs}$ (mas)	5.57 ± 0.28	6.44 ± 0.23
Hip97 π_{abs} (mas)	6.00 ± 0.67	5.74 ± 0.76
Hip07 π_{abs} (mas)	6.52 ± 0.77	5.01 ± 0.44
LKH Corr	-0.02	-0.01
$(m - M)_0$	6.29	6.00
M_V	-1.99 ± 0.11	$+1.18 \pm 0.08$
M_K	-3.52 ± 0.11	-0.26 ± 0.08

Note. [a] $V_t = 4.74 \times \mu / \pi_{abs}$.

included *X, Y* position within our total field of view; radial distance from the field-of-view center; reference star *V* magnitude and *B − V* color; and epoch of observation. We saw no obvious trends.

4.3.1. The Absolute Parallax of κ Pav

We constrain $\pi_x = \pi_y$ in Equations (3) and (4) and obtain for κ Pav a final absolute parallax $\pi_{abs} = 5.57 \pm 0.28$ mas. We have achieved a significant reduction in formal error, with the HIP97 determination, $\pi_{abs} = 6.00 \pm 0.67$ mas and the HIP07 determination, $\pi_{abs} = 6.52 \pm 0.77$ mas. A surface brightness (pulsation) parallax for κ Pav was determined by Feast et al. (2008) to be 4.90 ± 0.17 mas. The parallax of κ Pav derived in the present work is in better agreement with the pulsation parallax of Feast et al. (2008, a 2σ difference) than the HIP97 and HIP07 parallaxes. We note that this object is another for which the HIP07 re-reduction has not improved agreement with *HST*. See Barnes (2009) for a few other examples involving galactic Cepheids. Parallaxes and relative proper-motion results for all RRL and CP2 are collected in Tables 7 and 8.

4.3.2. Modeling Notes on the RRL and VY Pyx

Final model selection for all fields was based on reference star placement relative to the target, total number of reference stars, reduced χ^2 (χ^2/dof, where dof is the degrees of freedom), and parallax error. For all but the κ Pav, RR Lyr, and RZ Cep fields we increased the number of modeling coefficients in Equations (3) and (4) to six. We introduced radial terms, resulting in these equations of condition

$$\xi = Ax' + By' + G(x'^2 + y'^2)^{1/2} + C - \mu_x \Delta t - P_\alpha \pi_x \quad (6)$$

$$\eta = -Bx' + Ay' + H(x'^2 + y'^2)^{1/2} + F - \mu_y \Delta t - P_\delta \pi_y. \quad (7)$$

Absolute parallaxes, relative proper motions, and transverse velocities for κ Pav and associated reference stars are collected in Table 5. Parallaxes for all RRL and CP2 are collected in Tables 7 and 8.

All our absolute parallaxes directly rely on the estimates of reference star parallaxes. Should anyone wish to verify our results independently, the reference stars used in this study are all identified in archival material[21] held at the Space Telescope

---

[21] http://www.stsci.edu/observing/phase2-public/11211.pro

Table 8
RRL Parallaxes, Proper Motions, and Absolute Magnitudes

Parameter	XZ Cyg	UV Oct	RZ Cep	SU Dra	RR Lyr
Duration (yr)	2.87	2.38	2.41	2.52	13.14
Ref stars	4	5	4	5	5
Ref $\langle V \rangle$	13.68	14.75	14.88	14.70	13.75
Ref $\langle B - V \rangle$	0.78	0.85	1.04	0.70	0.71
$HST \mu$ (mas yr^{-1})	86.1 ± 0.1	133.4 ± 0.2	214.4 ± 0.3	90.7 ± 0.2	222.5 ± 0.1
P.A. ($^\circ$)	106.3 ± 0.2	205.8 ± 0.1	25.4 ± 0.1	210.9 ± 0.1	209.1 ± 0.1
V_t[a] (km s^{-1})	245 ± 22	368 ± 20	400 ± 27	307 ± 25	333 ± 13
$HST \pi_{abs}$ (mas)	1.67 ± 0.17	1.71 ± 0.10	2.12 ± 0.16	1.42 ± 0.16	3.77 ± 0.13
Hip97 π_{abs} (mas)	2.28 ± 0.86	1.48 ± 0.94	0.22 ± 1.09	1.11 ± 1.15	4.38 ± 0.59
Hip07 π_{abs} (mas)	2.29 ± 0.84	2.44 ± 0.81	0.59 ± 1.48	0.20 ± 1.13	3.46 ± 0.64
LKH Corr	-0.09	-0.03	-0.05	-0.11	-0.02
$(m - M)_0$	8.99	8.85	8.02	9.38	7.13
M_V	$+0.41 \pm 0.22$	$+0.35 \pm 0.13$	$+0.27 \pm 0.17$	$+0.40 \pm 0.25$	$+0.54 \pm 0.07$
M_K	-0.29 ± 0.22	-0.60 ± 0.13	-0.40 ± 0.16	-0.73 ± 0.25	-0.65 ± 0.07

Note. [a] Tangential velocity, $V_t = 4.74 \times \mu/\pi_{abs}$.

Science Institute. Adopted reference star spectral types for all fields are listed in Table 4.

XZ Cyg. Reference star 2 was removed from the data set because of high and unmodelable residuals. Application of Equations (6) and (7) to the remaining data resulted in a positional catalog with $\langle \sigma_\xi \rangle = 0.28$ and $\langle \sigma_\eta \rangle = 0.29$ mas. Residual histograms are well modeled with Gaussians of dispersion $\sigma_x = 1.4$ mas and $\sigma_y = 1.1$ mas. The resulting parallax, $\pi_{abs} = 1.67 \pm 0.17$ mas, agrees within the far larger errors of both the HIP97 and HIP07 value, $\pi_{abs} = 2.29 \pm 0.85$ mas.

UV Oct. Application of Equations (6) and (7) to these data resulted in a positional catalog with $\langle \sigma_\xi \rangle = 0.19$ and $\langle \sigma_\eta \rangle = 0.18$ mas. Residual histograms are well modeled with Gaussians of dispersion $\sigma_x = 1.0$ mas and $\sigma_y = 0.8$ mas. The resulting parallax, $\pi_{abs} = 1.71 \pm 0.10$ mas, is between the HIP97 ($\pi_{abs} = 1.48 \pm 0.94$ mas) and HIP07 ($\pi_{abs} = 2.44 \pm 0.81$ mas) values.

RZ Cep. Reference star 20 was removed from the data set because of high residuals. Application of Equations (4) and (5) to these data resulted in a positional catalog with $\langle \sigma_\xi \rangle = 0.37$ and $\langle \sigma_\eta \rangle = 0.37$ mas. Residual histograms are well modeled with Gaussians of dispersion $\sigma_x = 1.7$ mas and $\sigma_y = 1.2$ mas. The resulting parallax, $\pi_{abs} = 2.54 \pm 0.19$ mas differs from the HIP97 ($\pi_{abs} = 0.22 \pm 1.09$ mas) or HIP07 ($\pi_{abs} = 0.59 \pm 1.48$ mas) values. The *HST* value has a far smaller error.

SU Dra. Reference star 27 was removed from consideration because of high residuals. Application of Equations (6) and (7) to these data resulted in a positional catalog with $\langle \sigma_\xi \rangle = 0.34$ and $\langle \sigma_\eta \rangle = 0.39$ mas. Residual histograms have Gaussians with dispersion $\sigma_x = 0.9$ mas and $\sigma_y = 1.0$ mas. The resulting parallax, $\pi_{abs} = 1.42 \pm 0.16$ mas agrees within the larger errors of both HIP97 ($\pi_{abs} = 1.11 \pm 1.09$ mas) and HIP07 ($\pi_{abs} = 0.20 \pm 1.13$ mas), but is far more statistically significant.

RR Lyr. Because temporary onboard science-side failures left *HST* with few operational science instruments in late 2008, we were granted additional orbits for FGS astrometry. One of our targets was RR Lyr, a field for which we obtained five additional orbits. Application of Equations (4) and (5) to our original FGS 3 and these new data resulted in a positional catalog with $\langle \sigma_\xi \rangle = 0.34$ and $\langle \sigma_\eta \rangle = 0.52$ mas. Residual histograms are well fit with Gaussians of dispersion $\sigma_x = 0.7$ mas and $\sigma_y = 0.7$ mas. The resulting parallax, $\pi_{abs} = 3.77 \pm 0.13$ mas is between the HIP97 ($\pi_{abs} = 4.38 \pm 0.59$ mas) and HIP07 ($\pi_{abs} = 3.46 \pm 0.64$ mas) values. Our previous parallax value (Benedict et al. 2002b) was $\pi_{abs} = 3.82 \pm 0.20$ mas. The additional *HST* data have significantly improved the parallax and proper-motion precision compared to the 2002 values.

VY Pyx. Application of Equations (4) and (5) to these data resulted in a positional catalog with $\langle \sigma_\xi \rangle = 0.23$ and $\langle \sigma_\eta \rangle = 0.22$ mas. Residual histograms are well modeled with Gaussians of dispersion $\sigma_x = 1.4$ mas and $\sigma_y = 1.0$ mas. The resulting parallax, $\pi_{abs} = 6.44 \pm 0.23$ mas, is larger than both HIP97 ($\pi_{abs} = 5.74 \pm 0.76$ mas) and HIP07 ($\pi_{abs} = 5.01 \pm 0.44$ mas) values. We assessed the residuals from our modeling for evidence of orbital motion that could impact a parallax determination and found no significant signals. As done for all our modeling, we tested each spectrophotometrically determined reference star parallax by solving for a trigonometric parallax relative to the aggregate of reference stars and found no significant departures from the initial estimates. One last potential impact on a final parallax would be inadequate sampling of the parallactic ellipse. We show in Figure 5 the parallax factor coverage for both VY Pyx and RR Lyr. We are confident that our parallax is not affected by poor sampling of the parallactic ellipse of VY Pyx. We shall discuss this parallax result later in Section 5 when we determine absolute magnitudes and in Section 8, wherein we discuss both these peculiar CP2.

4.4. HST Parallax Accuracy

Our parallax precision, an indication of our internal, random error, is ∼0.2 mas. To assess our accuracy, or external error, we have compared (Benedict et al. 2002b; Soderblom et al. 2005) our parallaxes with results from independent measurements from *Hipparcos* (Perryman et al. 1997). See McArthur et al. (2011) for a more recent comparison with the *Hipparcos* re-reduction of van Leeuwen (2007). Other than for the Pleiades (Soderblom et al. 2005), we have no large systematic differences with *Hipparcos* for any objects with $\frac{\sigma_\pi}{\pi} < 10\%$. The next significant improvement in geometrical parallaxes for Population II variable stars will come from the space-based, all-sky astrometry missions *Gaia* (Lindegren et al. 2008) with ∼20 μas precision parallaxes. Final results are expected early in the next decade.
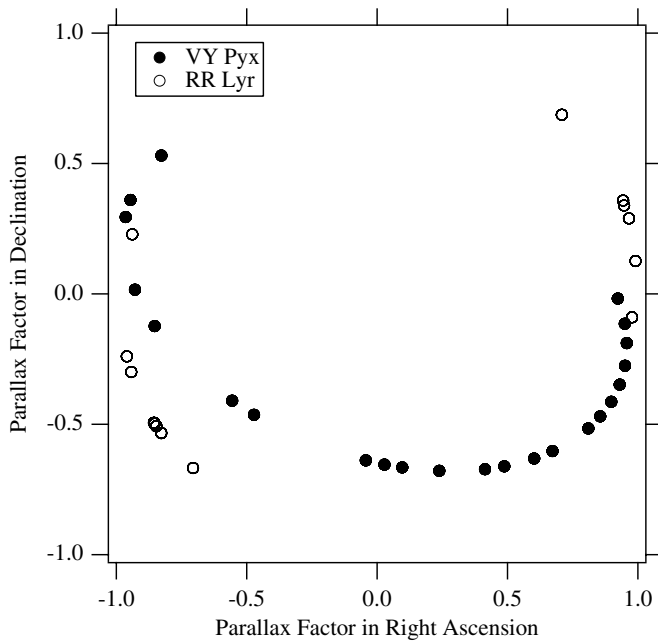
Figure 5. Sampling of the parallactic ellipses of VY Pyx and RR Lyr. Lack of coverage is not an issue in the parallax of VY Pyx.

5. THE ABSOLUTE MAGNITUDES OF THE RRL AND CP2

In using measured quantities involving distance, care has to be taken of bias questions. Lutz & Kelker (1973) in a well-known paper used a frequentist argument to show that if stars of the same measured parallax are grouped together, the derived mean parallax will be overestimated. This is because for most Galactic stellar distributions, the stars with overestimated parallaxes will outnumber those with underestimated parallaxes. This argument can be applied to single stars chosen by parallax and the argument can be put in a Bayesian form (see, for example, Section 5 of Benedict et al. 2007). There have been extensive discussions of the method in the literature (see, e.g., Smith 2003). Here we have used the general formulation of Hanson (1979) as applied to the determination of absolute magnitudes. The Lutz–Kelker–Hanson (LKH) bias in absolute magnitude is proportional to $(\sigma_\pi/\pi)^2$. Presuming that all RRL and CP2 in Table 2 belong to the same class of object (evolved Population II stars), we scale the LKH correction determined in Benedict et al. (2002b) for RR Lyr and obtain the LKH bias corrections listed in Tables 7 and 8. The average LKH bias correction for all objects in this study is -0.047 mag. We identify the choice of prior for this bias correction as a possible contributor to systematic errors in the zero points of our PLR at the 0.01 mag level. For our example target, κ Pav, we find LKH = -0.02 mag (Table 7). We have used these corrected absolute magnitudes in deriving zero points of the relations discussed below. In addition, we have used the uncorrected parallaxes to derived these zero points by the method of reduced parallaxes (RP). This RP approach avoids some of the bias problems (see Feast 2002, whose general scheme we use).

5.1. An Absolute Magnitude for κ Pav

With $\langle V \rangle = 2.78$ (Table 1) and given the absolute parallax, 5.57 ± 0.28 mas from Section 4.3.1, we determine a distance modulus for κ Pav. For all objects (except RZ Cep, where we adopt the Fernley et al. 1998 value) we adopt a color excess

from Feast et al. (2008), which for κ Pav (and an adopted $R = \frac{A_V}{E(B-V)} = 3.1$) yields $\langle A_V \rangle = 0.05$. With this $\langle A_V \rangle$, the measured distance to κ Pav, and the LKH correction we obtain $M_V = -1.99 \pm 0.11$ and a corrected true distance modulus, $(m - M)_0 = 6.29$. From the value in Feast et al. (2008), $\langle K_s \rangle = 2.78$ we obtain $M_K = -3.52 \pm 0.11$.

κ Pav has been identified to be a peculiar W Vir star (Feast et al. 2008; Feast 2010). See Section 8 for additional discussion. Results, including all proper motions and absorption- and LKH bias-corrected absolute magnitudes, for the objects in our program are collected for the CP2 in Table 7 and for the RRL in Table 8.

6. ZERO POINTS FOR THE RRL PERIOD–LUMINOSITY AND M_V–METALLICITY RELATIONS

6.1. The RRL M_K–log P Relation

A relation between K and $\log P$ for RRL was found by Longmore et al. (1986) in globular clusters. In more recent times a number of such relations have been suggested and these are given in Equations (8)–(13), where the zero points a_n refer to the mean period and metallicity of our parallax sample. The $\log P$ of RZ Cep, an overtone type "c" RRL, has been "fundamentalized" by adding +0.127, a factor determined by comparing type ab and type c RRLs, e.g., Oaster et al. (2006). Equation (8) was obtained by Sollima et al. (2008) from globular clusters with distance based on subdwarf parallaxes. Since the metallicity term is small, we also give the equation without the metallicity term (Equation (9)). Equation (10) is a semi-theoretical derivation. Equation (11) is from RRL in the cluster Reticulum in the LMC. Equation (12) was derived from RRLs of different metallicities in the globular cluster ω Cen, and Equation (13) is from RRL in the field of the LMC. For these relations the metallicities are all on, or close to, the Zinn–West system, except for Equation (8) where they are on the Carretta–Gratton (CG) system. The relations between different systems provided by Carretta & Gratton (1997) show that our mean ZW metallicity (-1.58) converts to -1.40 on the CG scale, and in view of the small size of the metallicity coefficient in Equation (8) the effect is negligible (~0.01 mag).

The values of a_n for these equations are listed in Table 9. Two values are given for each equation, one derived by fitting the LKH-corrected absolute magnitudes to the equation and one derived using the method of RP. The difference in the two zero points is within the uncertainties. Figure 6 shows a $K - \log P$ plot for our data. A slope of -2.38 (Equation (9)) was adopted for the fitted line. The CP2 κ Pav, included in the plot, will be discussed below (Section 8). It is not included in the fit.

The various PLR relationships and their sources are as follows.

$$M_K = (-2.38 \pm 0.04)(\log P + 0.28) + (0.08 \pm 0.11)$$
$$\times ([Fe/H] + 1.58) + a_1, \text{ Sollima et al. (2008)} \quad (8)$$

$$M_K = (-2.38 \pm 0.04)(\log P + 0.28) + a_2,$$
$$\text{Sollima et al. (2006), neglecting metallicity} \quad (9)$$

$$M_K = -2.101(\log P + 0.28) + (0.231 \pm 0.012)$$
$$\times ([Fe/H] + 1.58) + a_3, \text{ Bono et al. (2003)} \quad (10)$$

$$M_K = (-2.16 \pm 0.09)(\log P + 0.28) + a_4,$$
$$\text{Dall'Ora et al. (2004)} \quad (11)$$

Table 9
K and V Zero Points, a_n

n	λ	a(LKH)	a(RP)	b^a	c^b	Notes
1	K_s	-0.56 ± 0.02	-0.54 ± 0.03	-2.38	0.08	Sollima et al. (2008)
2	K_s	-0.57 ± 0.03	-0.54 ± 0.03	-2.38	...	Sollima et al. (2006), no [Fe/H]
3	K_s	-0.58 ± 0.04	-0.56 ± 0.04	-2.101	0.231	Bono et al. (2003)
4	K_s	-0.56 ± 0.02	-0.53 ± 0.04	-2.16	...	Dall'Ora et al. (2004)
5	K_s	-0.57 ± 0.02	-0.53 ± 0.03	-2.71	0.12	Del Principe et al. (2006)
6	K_s	-0.56 ± 0.03	-0.54 ± 0.03	-2.11	0.05	Borissova et al. (2009)
7	V	0.45 ± 0.05	0.46 ± 0.03	...	0.214	Gratton et al. (2004)

Notes.
^{a} $b = \log P$ coefficient.
^{b} $c = $ [Fe/H] coefficient.

$$M_K = (-2.71 \pm 0.12)(\log P + 0.28) + (0.12 \pm 0.04)$$
$$\times\ ([\text{Fe/H}] + 1.58) + a_5,\ \text{Del Principe et al. (2006)}\quad (12)$$

$$M_K = (-2.11 \pm 0.17)(\log P + 0.28) + (0.05 \pm 0.07)$$
$$\times\ ([\text{Fe/H}] + 1.58) + a_6,\ \text{Borissova et al. (2009)}.\quad (13)$$

6.2. An RRL M_V–[Fe/H] Relation Zero Point from HST Parallaxes

There is a long history of attempts to determine how M_V depends on [Fe/H]. A linear relation is generally assumed. Our data hint at a slope with the more metal-poor stars brighter. The best estimate for the slope (b) is probably from the work of Gratton et al. (2004), using RRL in the LMC ($b = 0.214$), and we have adopt that slope here. Figure 7 presents our M_V plotted against metallicity, [Fe/H], where the metallicity measures are from the sources noted in Table 1, all on the ZW scale. Fitting the function (Gratton et al. 2004)

$$M_V = (0.214 \pm 0.047)([\text{Fe/H}] + 1.5) + a_7 \quad (14)$$

to all RRLs, we obtain a zero point, $a_7 = +0.45 \pm 0.05$, listed in Table 9. Hence, $M_V = +0.45 \pm 0.05$ for RRLs with [Fe/H] $= -1.50$. The regression was carried out using GaussFit (Jefferys et al. 1988), which takes into account uncertainties along both axes. The rms of this fit, 0.08 mag in M_V, suggests an upper limit on the V-band cosmic dispersion in the absolute magnitudes of RRL. An RP approach finds $M_V = +0.46 \pm 0.03$. Note that the mean metallicity of our five RRLs, $\langle[\text{Fe/H}]\rangle = -1.58$, is so close to -1.50 that the error in the slope makes no significant difference to the zero point. Bono et al. (2007) find for field RRL a quadratic expression relating M_V to [Fe/H]; $M_V \propto 0.50[\text{Fe/H}] + 0.09[\text{Fe/H}]^2$. We fit (again with GaussFit) the distribution seen in Figure 7, constraining the [Fe/H] coefficients to the Bono et al. values and find a zero point $a = 0.98 \pm 0.05$. This and our average $\langle[\text{Fe/H}]\rangle = -1.58$ yield $\langle M_V\rangle = 0.42$, consistent with the Gratton et al. (2004) parameterization.

Regarding the intrinsic dispersion in RRL absolute magnitudes due to evolutionary effects, the intrinsic width of the RRL distribution in globular clusters near this metallicity has been shown by Sandage (1990) to be ± 0.2 mag. Thus, the standard deviation of a uniformly filled strip is 0.057. For five stars, the standard error we would find given such a strip (absent observational uncertainty) is 0.029 mag. Our observational uncertainty standard error for the five is 0.024 mag. Combine the two in quadrature and our claim of ± 0.05 mag is actually a bit conservative.
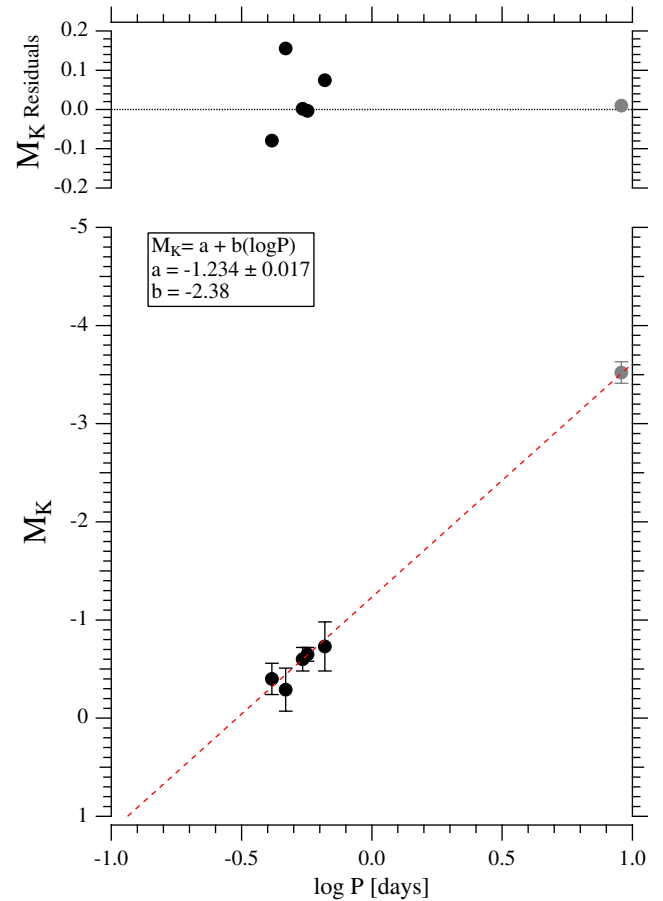
Figure 6. Population II K-band PLR. All magnitudes have been corrected for interstellar extinction. Coefficients are for $M_K = a + b \times (\log P)$. Zero-point (a) error is 1σ. The absolute magnitude (uncorrected for "peculiarity") and residual for κ Pav are plotted in gray. The fit is without κ Pav. The slope is constrained to $b = -2.38$ (Sollima et al. 2006). The largest residual is for XZ Cyg.
(A color version of this figure is available in the online journal.)

6.3. Comparison with Previous Determinations of RRL M_V and M_K

We compare in Table 10 past determinations of RRL M_V with our new value, $M_V = +0.45 \pm 0.05$ from LKH and $M_V = +0.46 \pm 0.03$ from the RP determination. An historical summary to the early 1990s is given by Smith (1995). Carretta et al. (2000 b), Cacciari & Clementini (2003), and Di Criscienzo et al. (2006) discuss more recent results.
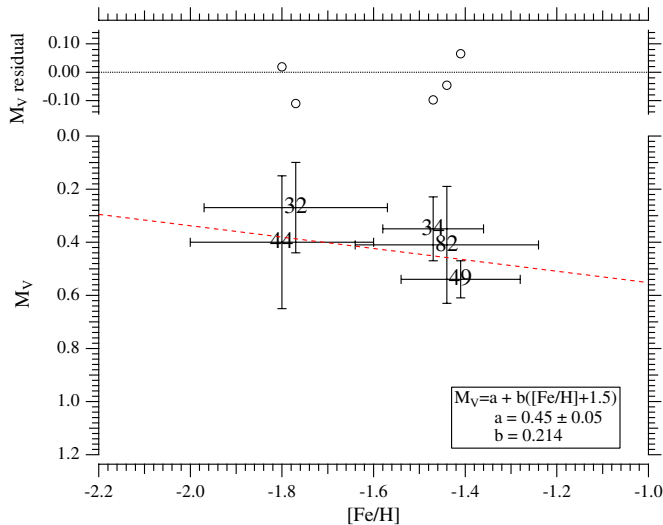
Figure 7. RRL extinction-corrected absolute magnitude M_V plotted against metallicity, [Fe/H], whose sources are given in Table 1. Objects are identified by model number: RZ Cep = 32; UV Oct = 34; SU Dra = 44; RR Lyr = 49; and XZ Cyg = 82. Errors in M_V and [Fe/H] are 1σ. The dashed line is an impartial fit to both the absolute magnitude and metallicity data with an adopted slope, b = 0.214 (Gratton et al. 2004), resulting in a zero point, a = +0.45 ± 0.05. The rms residual to this fit is 0.08 mag.

(A color version of this figure is available in the online journal.)

Table 10
RRL M_V at [Fe/H] = −1.5

M_V	Source[a]
0.45 ± 0.05	TP, this study, LKH
0.46 0.03	TP, this study, RP
0.40 0.22	TP, Koen & Laney (1998)
0.61 0.16[b]	TP, Benedict et al. (2002a, 2002b), Feast (2002)
0.47 0.12	GC, Carretta et al. (2000)
0.62 0.11	HB, Carretta et al. (2000)
0.75 0.13	SP, Gould & Popowski (1998)
0.55 0.12	SB, Cacciari & Clementini (2003)
0.68 0.05	Se, Fernley et al. (1998a)

Notes.
[a] SP: statistical parallax; GC: from subdwarf fits to globular clusters; HB: from trig parallax of field HB stars; SB: surface brightness; TP: trig parallax.
[b] Based on RR Lyrae only; includes an estimated cosmic dispersion component.

Four methods have generally been applied to the problem of Population II distances: trigonometric parallaxes, cluster-based distances, statistical parallaxes, and surface brightness analyses. In the following, we will use the absolute magnitude at [Fe/H] = −1.5 to inter-compare methods.

1. Trigonometric parallaxes are essentially free from complicating assumptions. However, one must still consider whether the instability region is sufficiently populated by the few data to give an unbiased relation. The first reliable parallax of an RRL came from the *Hipparcos* satellite. The Koen & Laney (1998) result is from an analysis of *Hipparcos* parallaxes of RRL. Fernley et al. (1998a) used the parallax for RR Lyr itself (with an adopted [Fe/H] = −1.39) of 4.38 ± 0.59 mas to estimate M_V = 0.78 ± 0.29 mag. *Hipparcos* also determined a distance to our target CP2 with 10%–13% errors. There are now two versions of the *Hipparcos* catalog: Perryman et al. (1997, HIP97) and van Leeuwen (2007, HIP07). We have reanalyzed the field for RR Lyr itself, which benefited from additional FGS data secured in late 2008. The Benedict et al. (2002b) *HST* parallax provided M_V = 0.61 ± 0.11, compared to our new value, M_V = 0.54 ± 0.07. Because the new and old parallaxes agree within their respective errors (Section 4.3.2), we ascribe the difference in M_V primarily to a newer and presumably more accurate extinction determination, A_V = 0.13 (Kolenberg et al. 2010). HIP97 and HIP07 parallaxes can be compared with the present *HST* results in Tables 7 and 8.

   Gratton (1998) derived an RRL scale based on the *Hipparcos* parallaxes of field horizontal-branch stars. The value in Table 10 is a slight update of this result (Carretta et al. 2000).

2. Cluster-based distances generally rely upon main-sequence or horizontal-branch fitting calibrated by stars with well-determined distances. Using *Hipparcos* parallaxes of 56 subdwarfs and data for nine globular clusters, Carretta et al.

(2000) obtain distances and hence the absolute magnitudes of the RRLs the clusters contain. Their result (Table 10) agrees well with ours, though their errors are large. Thus, our results promise improved accuracy in cluster distances.

3. Statistical parallaxes are derived by combining proper motions and radial velocities. Fernley et al. (1998b) performed such an analysis based on the *Hipparcos* proper motions. In an elaborate reanalysis of those data, Gould & Popowski (1998) confirmed the Fernley et al. result with a slightly smaller uncertainty. We quote the Gould & Popowski value in Table 10. There is about a 2σ difference from our value. This difference is not in itself of very high significance. However, the consequences of adopting RRLL absolute magnitudes 0.3 mag brighter than that suggested by the statistical parallaxes is highly important for distance scale applications. The reason for the fainter result obtained from statistical parallaxes is not clear. However, the statistical work depends on the adoption of a Galactic model. The result may be due to deviations from the adopted model (due possibly to stellar streams in the Galactic Halo). A full analysis of the Galactic motions of RRLs based on our new absolute magnitude scale is desirable.

   It is, however, interesting to note the work of Martin & Morrison (1998), who calculate the mean space motion (using radial velocities and proper motions) of Halo RRL with respect to the Sun as a function of the adopted absolute magnitude (their Figure 6). The velocity (V) in the direction of galactic rotation is quite sensitive to the absolute magnitude. For our derived value of the absolute magnitude scale their results predict V = −250 km s^{-1}. The galactic rotational velocity (with respect to the Sun) was recently determined from VLBI of Galactic masers (Brunthaler et al. 2011) as 246 ± 7 km s^{-1}. Our absolute magnitude scale implies that the halo RRL forms a non-rotating system. Both values of the galactic rotation were smaller and our result would have implied a retrograde halo. Lastly, Dambis (2009) obtained a calibration of a $K-\log P$ relation from statistical parallaxes which yields an $M_K \sim$ 0.4 mag fainter than our result. This suggests that the difference in M_V, comparing statistical parallaxes and our trigonometric work, is not due to problems with corrections for interstellar absorption.

4. Surface brightness extending the early efforts of Baade and Wesselink, Barnes & Evans (1976) introduced a technique for determining pulsating star distances using differential

Table 11
Globular Cluster Distance Moduli and Ages

ID	[Fe/H][a]	$E(B-V)$	λ	m_0	M_0	$(m-M)_0$	Ref.[b]	Age[c]
M3	-1.57	0.01	V	15.62 ± 0.05	0.45 ± 0.11	15.17 ± 0.12	1	
			K_s	13.93 ± 0.04	-1.23[d]	15.16 ± 0.06	2	10.8 ± 1.0
M4	-1.40	0.36	V	12.15 ± 0.06	0.47 ± 0.12	11.68 ± 0.13	3	
			K_s	10.97 ± 0.06	-0.52	11.48 ± 0.08	4	$11.1^{-1.4}_{+1.7}$
M15	-2.16	0.09	V	15.51 ± 0.05	0.32 ± 0.08	15.20 ± 0.09	5	
			K_s	14.67 ± 0.1	-0.52	15.18 ± 0.11	4	12.1 ± 1.0
M68	-2.08	0.04	V	15.51 ± 0.01	0.33 ± 0.08	15.18 ± 0.08	6	
			K_s	14.35 ± 0.04	-0.75	15.10 ± 0.06	7	12.4 ± 1.0
ω Cen	-1.84	0.11	V	14.2 ± 0.02	0.38 ± 0.09	13.82 ± 0.09	8	
			K_s	13.05 ± 0.06	-0.75	13.80 ± 0.08	9	. . .
M92	-2.16	0.025	V	15.01 ± 0.08	0.31 ± 0.08	14.70 ± 0.11	10	
			K_s	13.86 ± 0.04	-0.78	14.64 ± 0.06	11	13.1 ± 1.1

Notes.
[a] ZW scale.
[b] (1) Benkő et al. 2006; (2) Butler 2003; (3) Cacciari 1979; (4) Longmore et al. 1990, $\langle K \rangle$ and error estimated from Figure 1(c) at $\log P = -0.3$; (5) Silbermann & Smith 1995, Table 6, RRL ab only; (6) Walker 1994; (7) Dall'Ora et al. 2006; (8) Olech et al. 2003; (9) Del Principe et al. 2006, $\log P = -0.2$; (10) Kopacki 2001, Table 2, intensity-averaged V; (11) Del Principe et al. 2005, Table 3, RRL ab only, $\langle \log P \rangle = -0.19$.
[c] In Gyr.
[d] M_K errors, $\sigma = 0.05$ mag.

surface brightness measurements. There are two main uncertainties in the application of this general method to RRL. First, shocks occurring in the atmospheres of the stars during part of the pulsation cycle complicate the interpretation of the radial velocity curves. Second, it is necessary to adopt a value of p (the ratio of pulsation velocity to measured radial velocity) and this remains uncertain. Also, not all color indices are equally effective in predicting a surface brightness. The present status of the RRL M_V from this method is captured in the paper by Cacciari & Clementini (2003), who have introduced a number of refinements, but their work is for only one star, RR Cet. Our parallaxes may produce a more accurate p factor for RRL, and may refine p for CP2.

7. DISTANCE SCALE APPLICATIONS

We now apply our new zero points to several globular clusters and the LMC. The globular clusters were chosen because they had existing RRL photometry in both the V- and the K-band. We also estimate globular cluster ages with these new distance moduli. All parameterizations, sources of slopes, and zero points, and distance moduli derived from our new RRL absolute magnitudes listed in Table 8 and plotted in Figures 6 and 7 are summarized in Table 11 (Globular Clusters) and Table 12 (LMC). In each case we assume that $A_V = 3.1E(B-V)$ and $A_K = 0.11A_V$.

7.1. Distance Moduli of Globular Clusters

A sample of six globular clusters was selected based on the availability of both K-band and V-band RRL photometry. We first employ the zero point from M_K versus $\log P$, our Figure 6, comparing with the apparent magnitude PLR for each cluster. To each we also apply the M_V–[Fe/H] relation shown in Figure 7, transforming the relevant [Fe/H] from Sollima et al. (2006) on the CG scale to the ZW scale, using the CG–ZW mapping established by Carretta & Gratton (1997, their Equation (7)). The final M_V error includes the ± 0.047 mag M_V–[Fe/H] slope

Table 12
LMC Distance Moduli

Bandpass	$(m-M)_0$	Source
RRL		
K_s	18.55 ± 0.05	1
V	18.61 ± 0.05	2
V	18.46 ± 0.06	3
Reticulum Cluster RRL		
K_s	18.50 ± 0.03	4
Classical Cepheids		
V	18.52 ± 0.06	5
K	18.48 ± 0.04	5
W_{VI}	18.51 ± 0.04	5

Notes. The results for both the RRs and Cepheids are from LKH-corrected absolute magnitudes.
[1] LMC data from Borissova et al. (2009).
[2] LMC data from Gratton et al. (2004).
[3] LMC data from Soszynski et al. (2003).
[4] Reticulum cluster data from Dall'Ora et al. (2004).
[5] See Benedict et al. (2007).

error. The error in our adopted K-band PLR slope makes a negligible contribution to the final distance modulus error. The expectation is that the K and V distance moduli collected in Table 11 should agree. In all cases the two approaches yield the same distance modulus within the errors.

M3. From Benkő et al. (2006) we extract for RRL $\langle V_0 \rangle = 15.62 \pm 0.05$, corrected for an assumed $A_V = 0.03$. The Figure 7 M_V–[Fe/H] and an [Fe/H] $= -1.34$ (CG), [Fe/H] $= -1.57$ (ZW) provide $M_V = 0.45 \pm 0.05$, thus $(m-M)_0 = 15.17 \pm 0.12$. The Butler (2003) K-band apparent magnitude PLR zero point is 13.93 ± 0.04. This, combined with our Figure 6 zero point, yields $(m-M)_0 = 15.16 \pm 0.06$.

M4. For RRL Cacciari (1979) finds $\langle V_0 \rangle = 12.15 \pm 0.06$, corrected for an assumed $A_V = 1.19$. The Figure 7 M_V–[Fe/H] and an [Fe/H] $= -1.40$ (ZW) provide $M_V = 0.47 \pm 0.05$, thus $(m-M)_0 = 11.68 \pm 0.13$. The Longmore et al. (1990)

K-band apparent magnitude at $\log P = -0.3$ (Figure 1(f)) is $K(0) = 11.10 \pm 0.06$, corrected for $A_K = 0.13$. This, combined with our Figure 6 zero point, yields $(m - M)_0 = 11.48 \pm 0.08$. The two approaches barely yield the same distance modulus within the errors, possibly due to the high and uncertain extinction correction due to known differential reddening. We note that increasing to $E(B - V) = 0.415$ (from the adopted 0.36) equalizes the two distance moduli at $(m - M)_0 = 11.46$.

M15. From Silbermann & Smith (1995, Table 6), we derive $\langle V_0 \rangle = 15.51 \pm 0.02$, corrected for an assumed $A_V = 0.30$. This value comes only from the RRL ab stars. The Figure 7 M_V–[Fe/H] and an [Fe/H] $= -2.16$ (ZW) provide $M_V = 0.31 \pm 0.05$, thus $(m - M)_0 = 15.20 \pm 0.09$. The Longmore et al. (1990) K-band apparent magnitude at $\log P = -0.3$ (their Figure 1(c)) is $K_0 = 14.67 \pm 0.10$, corrected for $A_K = 0.03$. This, combined with our Figure 6 zero point, yields $(m - M)_0 = 15.18 \pm 0.11$.

M68. From Walker (1994) we obtain $\langle V_0 \rangle = 15.51 \pm 0.01$, corrected for an assumed $A_V = 0.13$. The Figure 7 M_V–[Fe/H] and an [Fe/H] $= -2.08$ (ZW) provide $M_V = 0.33 \pm 0.05$, thus $(m - M)_0 = 15.18 \pm 0.08$. The Dall'Ora et al. (2006) K-band apparent magnitude at $\log P = -0.2$ (their Figure 3) is $K_0 = 14.35 \pm 0.04$, corrected for $A_K = 0.01$. This, combined with our Figure 6 zero point, yields $(m - M)_0 = 15.10 \pm 0.06$.

ω Cen. Del Principe et al. (2006, Figure 4) provide $\langle K_0 \rangle = 13.05 \pm 0.06$ for RRL ab at $\log P = -0.2$. At that $\log P$ the Figure 6 PLR yields $M_K(0) = -0.75 \pm 0.05$. Hence, $(m - M)_0 = 13.80 \pm 0.08$. Adopting [Fe/H] $= -1.84$ (ZW), we obtain $M_V(0) = +0.38$ from Figure 7. RRL V-band photometry from Olech et al. (2003) and $A_V = 0.36$ (Sollima et al. 2006) provide $\langle V_0 \rangle = 14.20 \pm 0.02$ and $(m - M)_0 = 13.82 \pm 0.09$.

M92. From Kopacki (2001) we derive $\langle V_0 \rangle = 15.01 \pm 0.08$, corrected for an assumed $A_V = 0.08$. The Figure 7 M_V–[Fe/H] and an [Fe/H] $= -2.16$ (ZW) provide $M_V = 0.31 \pm 0.05$, thus $(m - M)_0 = 14.70 \pm 0.11$. The Del Principe et al. (2005) K-band apparent magnitude at $\log P = -0.19$ is $K_0 = 13.86 \pm 0.04$, corrected for $A_K = 0.01$. This, combined with our Figure 6 zero point, yields $(m - M)_0 = 14.64 \pm 0.06$. The two approaches yield the same distance modulus within the errors.

Within a year or so we will have an independent check on these globular cluster distance moduli. Chaboyer et al. (2011) are using the FGS on *HST* to obtain parallaxes of nine metal-poor ([Fe/H] < -1.5) main-sequence stars. The *HST* parallaxes are expected to have accuracies similar to those achieved for this RRL project, leading to absolute magnitude uncertainties of ± 0.05 mag for a given star. These stars will be used to test metal-poor stellar evolution models and to determine main-sequence fitting distances to a large number of low-metallicity globular clusters, including those above. See McArthur et al. (2011) for an example of the construction of a main sequence using only a few highly precise absolute magnitudes.

7.2. Globular Cluster Ages

Adopting the K-band distance moduli from Table 11, we calculate absolute ages for our selected globular clusters using a Monte Carlo simulation similar to that described by Chaboyer et al. (1998). We did not estimate an age for ω Cen, as the cluster is very complex with multiple stellar populations, and not conducive to a simple age determination. For each remaining globular cluster, 3000 sets of isochrones were generated using the Dartmouth stellar evolution program (Chaboyer et al. 2001; Bjork & Chaboyer 2006; Dotter et al. 2008). The input parame-

ters for each set of isochrones were randomly selected from their distribution function as discussed by Bjork & Chaboyer (2006). A total of 21 different parameters were varied in the stellar evolution calculations, including the nuclear reaction rates, opacities, surface boundary conditions, mixing length, and composition. The [Fe/H] values used in the stellar models were selected from a Gaussian distribution with a standard deviation of 0.15 dex and a mean based upon high-resolution spectroscopic abundance analysis of Fe I lines (Carretta et al. 2009) and Fe II lines (Kraft & Ivans 2003). These independent [Fe/H] measurements agree quite well with each for each of the globular clusters, and the mean of the two measurements were used in the stellar model calculations.[22]

The age of each globular cluster was determined using the absolute magnitude of the point on the subgiant branch which is 0.05 mag redder than the turnoff (Chaboyer et al. 1996). Photometry in V and I for each globular cluster except M15 was obtained from P. B. Stetson's photometric standard fields[23] and used to determine the apparent magnitude of the subgiant branch. The Stetson database for M15 does not reach the main-sequence turnoff in I. For this cluster, we used the *HST* Advanced Camera for Surveys photometry from Anderson et al. (2008). The V-band distance modulus for each cluster was determined using the true distance moduli (derived from the K band) and reddening listed in Table 11. Errors in the distance moduli were assumed to be Gaussian with the uncertainty given in Table 11, with the exception of M4. M4 has a fairly high reddening, and there is evidence for differential reddening across the clusters. Estimates for absorption in the V band range from $A_V = 1.16$ mag (using $E(B - V) = 0.36$ and the extinction calculator from McCall 2004) to $A_V = 1.33$ mag (Richer et al. 1997). We elected to use $A_V = 1.22 \pm 0.08$ mag, which implies an uncorrected $(m - M)_V = 12.70 \pm 0.11$ mag for M4. Lastly, the age error for M15 was derived from the smaller error on the V-band distance modulus.

We determined the ages (collected in Table 11) of the clusters as follows: M3, 10.8 ± 1.0 Gyr; M4, $11.1^{-1.4}_{+1.7}$ Gyr; M15, 12.1 ± 1.0 Gyr; M68, 12.4 ± 1.0 Gyr; and M92, 13.1 ± 1.1 Gyr. The larger error in the age of M4 is due to the larger uncertainty in the V-band distance modulus to this cluster.

Our absolute ages are in reasonable agreement with previous estimates. For example, di Cecco et al. (2010) found an absolute age of 11.0 ± 1.5 Gyr for M92, which agrees within the uncertainties with our age. The differences between our age estimate and that of di Cecco et al. (2010) is due our use of an updated nuclear reaction rate and a different distance modulus. di Cecco et al. (2010) used the older NACRE rate for the ^{14}N$(p, \gamma)^{15}$O nuclear reaction. We used the updated value for this critical nuclear reaction rate from Marta et al. (2008), which yields globular cluster ages approximately 1 Gyr older than the reaction rate used by di Cecco et al. di Cecco et al. (2010) adopted a distance modulus of 14.74 (no error reported), which is 0.1 mag larger than the distance modulus derived in this work. An increase in the distance modulus by 0.1 mag will decrease derived

_____

[22] The high-resolution spectroscopic [Fe/H] determinations for each cluster differ somewhat from the ZW scale listed in Table 11. Those [Fe/H] values were selected to be on the same [Fe/H] system as the target parallax stars (which, in general, do not have high dispersion spectroscopic [Fe/H] determinations). For the purposes of stellar model calculations, the consistency between the field stars and globular clusters stars is not an issue, rather one is interested in the absolute [Fe/H] scale, which is best determined from high-resolution spectroscopic studies.
[23] http://www4.cadc-ccda.hia-iha.nrc-cnrc.gc.ca/community/STETSON/ standards/

ages by approximately 1 Gyr. The distance modulus adopted by di Cecco et al. (2010) was the one that gave the best fit between their theoretical isochrones and the observed color–magnitude diagrams. It depends critically on their transformations for theoretical luminosities and temperatures to observed magnitudes and colors.

In general, it is difficult to find absolute age determinations for globular clusters in the literature. Most works focus on relative age determinations, and the errors in the age estimates do not include uncertainties in the stellar evolution models and isochrones. Although they focused on relative age determinations, Salaris & Weiss (2002) carefully determined the ages of a large sample of globular clusters, including all of the clusters whose ages are determined in this paper. The difference between our ages and those derived by Salaris & Weiss (2002) is within the errors: M92, 0.3 ± 1.4 Gyr; M68, 1.2 ± 1.3 Gyr; M3, -0.5 ± 1.2 Gyr; M15, 0.3 ± 1.4 Gyr; and M4, 0.1 ± 1.7 Gyr.

M3 is the only cluster we find to have a younger age than that derived by Salaris & Weiss (2002). This is likely due to the fact that the distance modulus we derive for this cluster is of order 0.1 mag larger than previous estimates, leading to our determination of a relatively young age for this cluster. Such a young age is supported by the fact that M3 has a relatively red horizontal-branch morphology for its metallicity. A detailed differential study of M3 and M13 (clusters with similar metallicities) by Rey et al. (2001) found that M3 was 1.7 ± 0.7 Gyr younger than M13. The biggest age difference between our work and Salaris & Weiss (2002) is for the globular cluster M68. Salaris & Weiss (2002) used [Fe/H] $= -2.00$ for this cluster, while we adopt [Fe/H] $= -2.33 \pm 0.15$ dex based upon more recent spectroscopic studies. Using [Fe/H] $= -2.00$ in our stellar evolution models reduces our age estimate for M68 by 1.1 Gyr to 11.3 Gyr and leads to good agreement with the Salaris & Weiss (2002) age estimate of this cluster of 11.2 Gyr.

7.3. LMC Distance Moduli

In this section, we derive the distance modulus of the LMC using our derived RRL absolute magnitudes. We then compare it with that derived from classical Cepheids, whose absolute magnitudes were also based on *HST* trigonometrical parallaxes (Benedict et al. 2007).

From observations of RRL in the LMC, Gratton et al. (2004) derived the relation

$$V_0 = (0.214 \pm 0.047)([Fe/H] + 1.5) + 19.064 \pm 0.017 \quad (15)$$

with metallicities on the ZW scale. This with the results in line 7 of Table 9 yields a true distance modulus of 18.61 ± 0.05 (Table 12) from the LKH approach. The OGLE team (Soszynski et al. 2003) found a mean value of $V_0 = 18.90 \pm 0.02$ for 7110 RRab and c stars in the LMC. This is from the OGLEII survey. The mean RRL magnitude (uncorrected for reddening) is not changed in the larger OGLEIII survey (Soszyński et al. 2009). Using the Gratton relation and adopting a mean metallicity of -1.53 for the LMC from Borissova et al. (2009) together with the zero points of Table 9 leads to an LMC modulus of 18.46 ± 0.06. The differences between these two results for the LMC modulus is primarily due to the fact that the two groups adopt different reddenings for the LMC objects (see Clementini et al. 2003).

For the infrared we have used the Borissova et al. (2009) work which has individual values of [Fe/H] and incorporates earlier work. Using Equation (13) with a zero point corresponding to

$a_6 = -0.54$ they obtain an LMC modulus of 18.53. The LK-corrected zero point in Table 9 then shows that our modulus is 0.02 mag brighter. We adopt 18.55 ± 0.05 based on the uncertainty of our zero point and the uncertainty in the infrared data. The result using the RP zero point is 18.53. The reddenings adopted by Borissova et al. were means of values derived in a variety of ways. The uncertainties in these values have a very small effect (of order 0.01 mag) on the derived distance modulus.

In view of the sensitivity of the derived LMC modulus to the reddening when using the relation in V, it seems best to give most weight to the determination using the relation in K. While we believe that this is the current best mean distance to the LMC from RR Lyraes, it should be noted that the LMC is sufficiently close that its depth structure is important. Thus strictly, the result applies to the selection of stars studied by Borissova et al. and the model of the LMC that they adopt. A similar remark applies to other determinations.

Dall'Ora et al. (2004) established a K-band PLR in the Reticulum cluster associated with the LMC:

$$K_0 = -2.16 \log P + 17.33 \pm 0.03. \quad (16)$$

This, together with a_4 in Table 9, leads to a corrected distance modulus for the cluster of 18.50 ± 0.03. As discussed by Dall'Ora et al. the relative distance of this cluster and the main body of the LMC has not been well established. Our result suggests that any difference in distance is small.

In view of the above discussion, we adopt 18.55 ± 0.05 (LKH method) or 18.53 (RP method) as the best RRL distance to the LMC. This may be compared with the LMC modulus obtained by Benedict et al. (2007) from classical Cepheids based on *HST* parallaxes of Galactic stars of this type. Their results were $(m - M)_0 = 18.50 \pm 0.04$ from a PL relation in W_{VI}; 18.52 ± 0.06 from a PL relation in V_0: and 18.48 ± 0.04 from a PL relation in K_0. These results have not been corrected for the metallicity difference between the LMC Cepheids and the Galactic calibrating stars. There has been much discussion as to whether or not a metallicity correction to Cepheid absolute magnitudes is necessary. The above results show that any correction is small, at least between Cepheids of Galactic and LMC metallicities. This result agrees with the theoretical discussion of Bono et al. (2010).

We note that recent work (Laney & Pietrzyński 2009) on the absolute magnitude calibration of red clump stars, which formerly led to a rather low modulus for the LMC, now gives $(m - M)_0 = 18.47 \pm 0.03$ in good agreement with the RRL and (uncorrected for metallicity) Cepheid results.

8. THE TYPE 2 CEPHEIDS

In this section, we discuss the two CP2s for which we have obtained parallaxes and absolute magnitudes. Matsunaga et al. (2006) established an $M_K - \log P$ relation for CP2s in globular clusters which shows little evidence of a metallicity dependence. It was therefore originally anticipated that the parallaxes of these two stars, κ Pav ($\log P = 0.958$) and VY Pyx ($\log P = 0.093$), could be used to establish a zero point for this relation, which appears to be continuous with a PL relation for RRLs. Subsequent work (Soszyński et al. 2009; Matsunaga et al. 2009) has shown that in the LMC field the situation is more complex than in globular clusters. Some CP2 with periods near that of κ Pav lie above the PL relation and have distinctive light curves (peculiar W Vir stars). Many of these stars are known to be binaries. It has now been suggested (Feast et al. 2008) that

κ Pav belongs to this class, though it is not known to be binary and the classification remains uncertain.

The identification of a star as belonging to an older stellar population can be based on kinematics and/or metallicity. The RRL transverse velocities, V_t in Table 8, all suggest an identification with the halo, or that these stars have no connection with the local stellar thin disk population. As summarized in Maas et al. (2007), the identification of CP2 is more complex. First, there is separation by period and metallicity. The prototype short-period CP2 is BL Her with $P = 1^d31$ and [Fe/H] $= -0.1$ (Maas et al. 2007). The long-period prototype CP2 is W Vir with $P = 17.27$ days and [Fe/H] $= -1.0$ (Barker et al. 1971). In addition to detailed metallicity variations by species the classification of CP2 also rests on distance from the Galactic plane, $|Z|$. The Galactic latitudes of VY Pyx and κ Pav, $+13°6$ and $-25°4$, respectively, together with the Table 7 parallaxes, yield Z values of 36.5 pc and 77 pc, not particularly extreme. Nor are the transverse velocities of VY Pyx and κ Pav (Table 7) indicative of halo or thick disk membership. The metallicity of κ Pav, [Fe/H] $= 0.0$ (Luck & Bond 1989), is far from the prototypical [Fe/H] $= -1$. In contrast, our newly measured metallicity for VY Pyx ([Fe/H] $= -0.01$, Table 1) is the same as that measured by Maas et al. (2007) for the prototype BL Her (though their value for VY Pyx is -0.4).

Figure 6 shows an $M_K - \log P$ relation. The slope (-2.38 ± 0.04) was derived by Sollima et al. (2006) from RRLs in globular clusters. This is essentially the same as the slope found by Matsunaga et al. (2006) for CP2s in globular clusters (-2.41 ± 0.05). The zero point was fixed by our RRLs which are shown. This relation passes within 0.01 mag of our absolute magnitude of κ Pav, which is also plotted, although this star was not used in deriving the zero point. This suggests that either κ Pav is not a peculiar W Vir star, or is one of the few that lie near the PL relation. It is very desirable to clear up this matter. If it can be used as a normal CP2, it would add significantly to the distance scale calibration.

VY Pyx at M_K, $\log P = -0.26$, 0.0934 lies $+1.19 \pm 0.08$ mag below the regression line of Figure 6. A weighted average of HIP97 and HIP07 parallaxes ($\pi_{abs} = 5.37 \pm 0.38$) gives $M_K = -0.68 \pm 0.16$, which is $+0.78$ mag below the regression line. It is not clear whether this star indicates that a wide range of absolute magnitudes is possible for short-period CP2s, or whether it is a rare anomaly. Detailed studies of CP2s with periods near one day in the Magellanic Clouds may answer this question.

9. SUMMARY

1. *HST* astrometry has now yielded absolute trigonometric parallaxes for five RRL variables and two CP2s with an average $\sigma_\pi = 0.18$ mas, or $\sigma_\pi/\pi = 5.4\%$. These parallaxes, along with precision photometry culled from the literature, LKH bias corrections, and reddening corrections derived from both the literature and/or our ancillary spectrophotometry, provide absolute magnitudes with which to extract zero points for a PLR and an M_V–[Fe/H] relation. The restricted ranges of both $\log P$ and [Fe/H] preclude solving for slopes. Adopting previously determined slopes, our zero-point errors are now at or below 0.03 mag in the K bandpass and 0.05 in the V bandpass.

2. To obtain these parallaxes, no RRL or CP2 required the addition of a perturbation orbit in the modeling.

3. The CP2 κ Pav ($\log P = 0.96$) lies within 0.01 mag of the value predicted by an extrapolation of an RRL $K_s - \log P$ relation based on a slope derived from globular clusters and our parallax zero point. This star could be an important distance scale calibrator if the uncertainty regarding its nature (normal or peculiar CP2) can be resolved. This situation appears to support the assertion that RRL and CP2 together can establish a single PLR (Matsunaga et al. 2006; Majaess 2010).

4. Our absolute magnitude of the CP2 star VY Pyx ($\log P = 0.093$) falls well below a $K_s - \log P$ relation for RRLs based on our zero point. This result is not currently understood but we see no reason to question the accuracy of our parallax.

5. We apply our V and K calibrations to selected galactic globular clusters. We obtain K-band PLR and M_V–[Fe/H] distance moduli that agree within the errors for all clusters. Ages obtained from stellar evolution models range 10.8–13.1 Gyr.

6. Based on the K_s–[Fe/H]–$\log P$ relation of Borissova et al. (2009) and with our zero-point calibration, we derive an LMC distance modulus of $(m - M)_0 = 18.55 \pm 0.05$. This result agrees within the errors with that derived from classical Cepheids, calibrated by *HST* parallaxes (Benedict et al. 2007), and uncorrected for metallicity differences between the Galactic calibrators and the LMC Cepheids.

for careful reading and extensive constructive criticism that
materially improved the presentation and discussion.

REFERENCES

Alcock, C., Alves, D. R., Becker, A., et al. 2003, ApJ, 598, 597
Anderson, J., Sarajedini, A., Bedin, L. R., et al. 2008, AJ, 135, 2055
Barcza, S. 2002, A&A, 384, 460
Barker, T., Baumgart, L. D., Butler, D., et al. 1971, ApJ, 165, 67
Barnes, T. G. 2009, in AIP Conf. Proc. 1170, Stellar Pulsation: Challenges for
    Theory and Observation, ed. J. A. Guzik & P. A. Bradley (Melville, NY:
    AIP), 3
Barnes, T. G., & Evans, D. S. 1976, MNRAS, 174, 489
Benedict, G. F., McArthur, B. E., Bean, J. L., et al. 2010, AJ, 139, 1844
Benedict, G. F., McArthur, B. E., Feast, M. W., et al. 2007, AJ, 133, 1810
Benedict, G. F., McArthur, B. E., Fredrick, L. W., et al. 2002a, AJ, 124, 1695
Benedict, G. F., McArthur, B. E., Fredrick, L. W., et al. 2002b, AJ, 123, 473
Benedict, G. F., McArthur, B., Nelan, E., et al. 1998, AJ, 116, 429
Benkő, J. M., Bakos, G. Á., & Nuspl, J. 2006, MNRAS, 372, 1657
Bessell, M. S., & Brett, J. M. 1988, PASP, 100, 1134
Bjork, S. R., & Chaboyer, B. 2006, ApJ, 641, 1102
Bono, G., Caputo, F., Castellani, V., et al. 2003, MNRAS, 344, 1097
Bono, G., Caputo, F., & Di Criscienzo, M. 2007, A&A, 476, 779
Bono, G., Caputo, F., Marconi, M., et al. 2010, ApJ, 715, 277
Borissova, J., Rejkuba, M., Minniti, D., et al. 2009, A&A, 502, 505
Brunthaler, A., Reid, M. J., Menten, K. M., et al. 2011, Astron. Nachr., 332, 461
Butler, D. J. 2003, A&A, 405, 981
Cacciari, C. 1979, AJ, 84, 1542
Cacciari, C., & Clementini, G. 2003, in Stellar Candles for the Extragalactic
    Distance Scale, ed. D. Alloin & W. Gieren (Lecture Notes in Physics, Vol.
    635; Berlin: Springer), 105
Cacciari, C., Corwin, T. M., & Carney, B. W. 2005, AJ, 129, 267
Carretta, E., Bragaglia, A., Gratton, R., et al. 2009, A&A, 508, 695
Carretta, E., & Gratton, R. G. 1997, A&AS, 121, 95
Carretta, E., Gratton, R. G., & Clementini, G. 2000, MNRAS, 316, 721
Chaboyer, B. C., Benedict, G. F., McArthur, B. E., et al. 2011, BAAS, 217,
    242.45
Chaboyer, B., Demarque, P., Kernan, P. J., et al. 1996, MNRAS, 283, 683
Chaboyer, B., Demarque, P., Kernan, P. J., et al. 1998, ApJ, 494, 96
Chaboyer, B., Fenton, W. H., Nelan, J. E., et al. 2001, ApJ, 562, 521
Clementini, G., Gratton, R., Bragaglia, A., et al. 2003, AJ, 125, 1309
Cox, A. N. 2000, Allen's Astrophysical Quantities (4th ed.; New York: AIP
    Press)
Dall'Ora, M., Bono, G., Storm, J., et al. 2006, Mem. Soc. Astron. Italiana, 77,
    214
Dall'Ora, M., Storm, J., Bono, G., et al. 2004, ApJ, 610, 269
Dambis, A. K. 2009, MNRAS, 396, 553
Del Principe, M., Piersimoni, A. M., Bono, G., et al. 2005, AJ, 129, 2714
Del Principe, M., Piersimoni, A. M., Storm, J., et al. 2006, ApJ, 652, 362
di Cecco, A., Becucci, R., Bono, G., et al. 2010, PASP, 122, 991
Di Criscienzo, M., Caputo, F., Marconi, M., et al. 2006, MNRAS, 365, 1357
Dotter, A., Chaboyer, B., Jevremović, D., et al. 2008, ApJS, 178, 89
Epps, E. A., & Sinclair, J. E. 1973, Observatory, 93, 78
Feast, M. 2002, MNRAS, 337, 1035
Feast, M. W. 2010, in Variable Stars, the Galactic Halo and Galaxy Formation,
    ed. C. Sterken, N. Samus, & L. Szabados (Moscow: Sternberg Astronomical
    Institute), 45
Feast, M. W., Laney, C. D., Kinman, T. D., et al. 2008, MNRAS, 386, 2115
Fernley, J., Barnes, T. G., Skillen, I., et al. 1998a, A&A, 330, 515
Fernley, J., Skillen, I., Carney, B. W., et al. 1998b, MNRAS, 293, L61
Gould, A., & Morgan, C. W. 2003, ApJ, 585, 1056
Gould, A., & Popowski, P. 1998, ApJ, 508, 844
Gratton, R. G. 1998, MNRAS, 296, 739
Gratton, R. G., Bragaglia, A., Clementini, G., et al. 2004, A&A, 421, 937
Hanson, R. B. 1979, MNRAS, 186, 875
Hardie, R. H. 1955, ApJ, 122, 256
Holtzman, J. A., Harrison, T. E., & Coughlin, J. L. 2010, Adv. Astron., 2010,
    46

Jefferys, W. H., Fitzpatrick, M. J., & McArthur, B. E. 1988, Celest. Mech., 41,
    39
Koen, C., & Laney, D. 1998, MNRAS, 301, 582
Kolenberg, K., Fossati, L., Shulyak, D., et al. 2010, A&A, 519, 64
Kolenberg, K., Smith, H. A., Gazeas, K. D., et al. 2006, A&A, 459, 577
Kopacki, G. 2001, A&A, 369, 862
Kraft, R. P., & Ivans, I. I. 2003, PASP, 115, 143
LaCluyzé, A., Smith, H. A., Gill, E., et al. 2004, AJ, 127, 1653
Laney, C. D., & Pietrzyński, G. 2009, in AIP Conf. Ser. 1170, Stellar Pulsation:
    Challenges for Theory and Observation, ed. J. A. Guzik & P. A. Bradley
    (Melville, NY: AIP), 34
Layden, A. C. 1994, AJ, 108, 1016
Lindegren, L., Babusiaux, C., Bailer-Jones, C., et al. 2008, in IAU Symp. 248,
    A Giant Step: from Milli- to Micro-arcsecond Astrometry, ed. W. J. Jin, I.
    Platais, & M. A. C. Perryman (Cambridge: Cambridge Univ. Press), 217
Longmore, A. J., Dixon, R., Skillen, I., et al. 1990, MNRAS, 247, 684
Longmore, A. J., Fernley, J. A., & Jameson, R. F. 1986, MNRAS, 220, 279
Luck, R. E., & Bond, H. E. 1989, ApJ, 342, 476
Lutz, T. E., & Kelker, D. H. 1973, PASP, 85, 573
Maas, T., Giridhar, S., & Lambert, D. L. 2007, ApJ, 666, 378
Majaess, D. J. 2010, J. Am. Assoc. Var. Star Obs., 38, 100
Marta, M., Formicola, A., Gyürky, G., et al. 2008, Phys. Rev. C, 78, 022802
Martin, J. C., & Morrison, H. L. 1998, AJ, 116, 1724
Matsunaga, N., Feast, M. W., & Menzies, J. W. 2009, MNRAS, 397, 933
Matsunaga, N., Fukushi, H., Nakada, Y., et al. 2006, MNRAS, 370, 1979
McArthur, B. E., Benedict, G. F., Harrison, T. E., et al. 2011, AJ, 141, 172
McArthur, B., Benedict, G. F., Jefferys, W. H., et al. 2002, in The 2002 *HST*
    Calibration Workshop: Hubble After the Installation of the ACS and the
    NICMOS Cooling System, ed. S. Arribas, A. Koekemoer, & B. Whitmore
    (Baltimore, MD: STScI), 373
McArthur, B. E., Benedict, G. F., Lee, J., et al. 2001, ApJ, 560, 907
McCall, M. L. 2004, AJ, 128, 2144
Nelan, E. P. 2010, Fine Guidance Sensor Instrument Handbook (17th ed.;
    Baltimore, MD: STScI)
Oaster, L., Smith, H. A., & Kinemuchi, K. 2006, PASP, 118, 405
Olech, A., Kaluzny, J., Thompson, I. B., et al. 2003, MNRAS, 345, 86
Perryman, M. A. C., Lindegren, L., Kovalevsky, J., et al. 1997, A&A, 323,
    L49
Rey, S. C., Yoon, S. J., Lee, Y. W., et al. 2001, AJ, 122, 3219
Richer, H. B., Fahlman, G. G., Ibata, R. A., et al. 1997, ApJ, 484, 741
Roeser, S., Demleitner, M., & Schilbach, E. 2010, AJ, 139, 2440
Salaris, M., & Weiss, A. 2002, A&A, 388, 492
Sandage, A. 1990, ApJ, 350, 603
Sanwal, N. B., & Sarma, M. B. K. 1991, JA&A, 12, 119
Savage, B. D., & Mathis, J. S. 1979, ARA&A, 17, 73
Schlegel, D. J., Finkbeiner, D. P., & Davis, M. 1998, ApJ, 500, 525
Shobbrook, R. R. 1992, MNRAS, 255, 486
Silbermann, N. A., & Smith, H. A. 1995, AJ, 110, 704
Smith, H. A. 1995, RR Lyrae Stars (Cambridge: Cambridge Univ. Press)
Smith, H. 2003, MNRAS, 338, 891
Soderblom, D. R., Nelan, E., Benedict, G. F., et al. 2005, AJ, 129, 1616
Sollima, A., Cacciari, C., Arkharov, A. A. H., et al. 2008, MNRAS, 384,
    1583
Sollima, A., Cacciari, C., & Valenti, E. 2006, MNRAS, 372, 1675
Soszynski, I., Udalski, A., Szymanski, M., et al. 2003, Acta Astron., 53, 93
Soszyński, I., Udalski, A., Szymański, M. K., et al. 2009, Acta Astron., 59, 1
Standish, E. M., Jr. 1990, A&A, 233, 252
Sturch, C. 1966, ApJ, 143, 774
Subasavage, J. P., Bailyn, C. D., Smith, R. C., et al. 2010, Proc. SPIE, 7737,
    31
van Altena, W. F., Lee, J. T., & Hoffleit, E. D. 1995, The General Catalogue
    of Trigonometric [Stellar] Parallaxes (4th ed.; New Haven, CT: Yale Univ.
    Observatory) (YPC95)
van Leeuwen, F. 2007, *Hipparcos*, the New Reduction of the Raw Data
    (Astrophysics and Space Science Library, Vol. 350; Berlin: Springer)
Walker, A. R. 1994, AJ, 108, 555
Yong, D., & Lambert, D. L. 2003, PASP, 115, 796
Zakrzewski, B., Ogloza, W., & Moskalik, P. 2000, Acta Astron., 50, 387
Zinn, R., & West, M. J. 1984, ApJS, 55, 45